International Journal of Plasticity 30–31 (2012) 18–40

Contents lists available at SciVerse ScienceDirect

International Journal of Plasticity

journal homepage: www.elsevier.com/locate/ijplas

Instability criterion of materials in combined stress states and its application to orthogonal cutting process

Wei Ma *, Xiangwang Li, Lanhong Dai, Zhong Ling

Institute of Mechanics, Chinese Academy of Sciences, Beijing 100190, China

ARTICLE INFO

Article history:
Received 8 April 2011
Received in final revised form 26 August 2011
Available online 22 September 2011

Keywords:
Instability criterion
A. Plastic collapse
A. Cutting and forming
C. Asymptotic analysis
A. Thermomechanical processes

ABSTRACT

The loadings of variable combined stresses may cause different instabilities of materials such as the shear localization instability or non-localized thermal softening instability. The purpose of this paper is to present a theoretical analysis of instability behaviors of material under the loading conditions of combined stresses and apply the analytical results to interpret the removal mechanisms of chip materials in cutting process. First, the perturbation analysis of material instability under the loading conditions of combined stresses and relatively critical conditions are presented, followed by discussions on relations between the instability behaviors of materials and the loading conditions. Then, the removal mechanisms of chip materials in cutting process are studied by numerical simulation. The formation of continuous and discontinuous chips is shown closely related to the plastic flow and instability behaviors of the chip material, and the transformation between the two types of chips is found dependent on the ratio of plastic work dissipated by dilatation deformation and that dissipated by shear deformation.

1. Introduction

There are many instable modes for materials when the loading conditions are variable. Shear band is an instable mode of localized plastic deformation. Usually, shear band occurs in a narrow deformation zone in which material subjects to high intensity shear and large temperature rise. Hence, shear band is often called as the localized thermal softening instability. In a different way, necking in the simple tension case is another instable mode and takes place in a relatively large deformation zone compared with the shear banding case, and thus is called as non-localized thermal softening instability. If no instability occurs, the deformation behavior of materials is somewhat a steady homogeneous plastic flow. So far, many studies have shown that the instability of materials depends on both the thermophysical and mechanical properties of materials and the loading conditions. However, no major studies have been conducted on whether the instability occurs in the form of localized thermal softening or non-localized thermal softening under the loading conditions of complex stresses (Anand et al., 1987; Zbib and Jubran, 1992; Batra and Liu, 1990), and thus, for some engineering fields as metal machining, it is not easy to provide a logical prediction on the instability behaviors of materials and the transition between different instability modes. Therefore, it is necessary to further study the instability behaviors of materials under complex stresses loading conditions.

In the last several decades, shear localization instability has received considerable attention in academic community. For determining the critical conditions of shear band formation, some researchers, such as Argon (1973), Culver (1973) and Staker (1981), proposed an instability criteria based on the maximum shear stress to estimate the shear banding instability in homogeneous material deformation. Others (Clifton, 1980; Bai, 1982; Burns and Trucano, 1982; Pan, 1983) established

* Corresponding author. Address: 15 Beisihuan West Road, Beijing 100190, China. Tel./fax: +86 01 82544238.
E-mail address: watwm@imech.ac.cn (W. Ma).

0749-6419/$ - see front matter © 2011 Elsevier Ltd. All rights reserved.
doi:10.1016/j.ijplas.2011.09.003

instability criteria for the shear localization instability by using linear perturbation method. Bai's study (1982) showed that the shear localization instability was related to the thermal softening, current stress, specific heat and work hardening, but almost not to the heat conduction. By linear perturbation analysis, he established the adiabatic instability criterion of thermoplastic materials in the simple shear case. In order to study the influence of material properties, initial imperfections and boundary conditions on the deformation localization instability of materials, Fressengeas and Molinary (1987) studied the unsteadiness of homogeneous plastic flow of materials and provided a long range instability prediction with relative perturbation method. Anand et al. (1987) carried out a three-dimensional perturbation analysis for the shear localization instability. For the cases of quasi-static isothermal deformation and dynamic adiabatic deformation of viscoplastic materials, they established the onset conditions for the formation of shear bands and determined the probable directions of shear bands evolution. Especially, they studied the effect of pressure hardening on shear banding instability behaviors.

In recent years, many studies were performed on the mechanism underlying the localization instability of materials and the formation of shear bands (e.g. Kuroda, 1996; Kuroda and Tvergaard, 2007; Hashiguchi and Tsutsumi, 2007; Borg, 2007; Farrokh and Khan, 2009; Paul et al., 2009; Kobayashi, 2010; Chen and Lin, 2010; Mroginski et al., 2011; Sun et al., 2009). Kuroda (1996) studied the softening effect on the development of shear bands by using different types of plastic constitutive models with plastic spin. He found that, the stress rate dependent non-coaxial model described the geometric softening and could not predict the shear band formation. The strain-softening model predicted the effects of material softening and the geometric softening arising from the back stress. For the porous model, the material softening due to the pressure-sensitive void damage was a dominant factor, inducing the localized deformation. In the study of the effects of texture components on shear band formation in plane strain tension/compression and bending, Kuroda and Tvergaard (2007) found that the critical strain at the onset of shear banding and the corresponding orientation of shear band were two key quantities affecting shear band formation, and cube texture advantageously prevented the shear band development. Hashiguchi and Tsutsumi (2007), based on gradient plasticity constitutive model, performed the post-localization analysis of granular materials to predict the shear band thickness. They found that the gradient coefficient characterizing the inhomogeneity of deformation determined the shear-band thickness. Borg (2007) studied the effect of internal material length scale on the localization of plastic flow in shear bands in a single crystal under plane strain tension. It was shown that there was little mesh sensitivity when the nonlocal material model was used. Furthermore, it was found that increasing the material length scale delayed the formation of shear bands. Also, Niordson and Tvergaard (2005) investigated the instability behaviors for tension and compression specimens using a rate-independent strain gradient plasticity theory and observed the effect of material length scale on the necking behavior. The study by Paul et al. (2009) on twinning and shear banding in a plane strain Cu–Al alloy single crystal showed that the texture changes were only due to one kind of deformation twinning. It was shown that, at larger deformations, twin matrix deflection within some narrow areas led to kink-type bands as the precursors of shear bands. Short distance dislocation movement led to local lattice rotation and to kink-type shear bands. Long distance dislocation slip across the entire crystal thickness led to strain accommodation on a macroscopic scale. Moreover, the reorientation of the twinning planes towards the shear band plane promoted dislocation slip in the shear banding direction. In the study of ductile failure of dual phase steels (Sun et al., 2009), the microstructure-level inhomogeneity serving as the initial imperfection was found to trigger the instability in the form of plastic strain localization during the deformation process, showing that the local failure mode and ultimate ductility were related to the stress states. A dominant shear band led to material failure under the plane stress condition, while necking led to the material failure under plane strain loading condition. Kobayashi (2010) analyzed the deformation localization behaviors based on the theory of ultrasonic wave propagating in plastic materials, and obtained the diagrams of diffuse necking, localized necking and the formation of limit conditions. More recently, many investigations on deformation localization behaviors showed a tendency toward extended material models. For example, some studies focused on the formation of shear bands in bulk metallic glasses (Jiang and Dai, 2009; Chen and Lin, 2010), and others dealt with the localized failure modes of porous media (Di Rado et al., 2009; Mroginski et al., 2011).

Instability of materials in the shear localization deformation, especially in high speed cutting process, is still an open question, and further profound and extensive investigations of the physical mechanism underlying shear deformation localization is helpful to clarify the removal mechanism of chip materials from the workpiece surfaces. Experimental observations of the chip morphologies (Komanduri, 1982; Sutter et al., 1997; Molinari et al., 2002) showed that continuous and discontinuous or segmented chips developed in cutting process. In particular, the shear bands are widely observed in the discontinuous chip, which lays a foundation for studying the cutting mechanisms of materials theoretically and numerically. In the studies of the physical mechanisms of discontinuous chip formation, one-dimensional cutting model is widely used. The "deck of cards" model of material machining (Piispanen, 1948) describes morphologically the removal mechanisms of thin lamella materials on workpiece surfaces and the adiabatic shear band formation between the thin lamellae in orthogonal cutting process. Merchant (1945) analyzed the geometry of continuous and discontinuous chips and the interaction forces between chip and tool in the orthogonal cutting, providing a useful insight into the nature of cutting process. Recht's study (1964) showed that catastrophic shear failure occurred when the thermal softening effect surpassed the strain hardening effect, and repeated formation of shear bands in chip materials resulted in the occurrence of segmental chips. Plastic slip is the influential deformation mechanism of chip materials in cutting process. The decrease of cutting speeds results in the decrease of temperature gradients and the reduction of the spacing between shear bands in chip materials. When steady plastic flow occurs, the spacing band approaches to zero and continuous chips take form. Recent study performed by Burns and Davies (2002) revealed that the interaction compression between tool and workpiece and the tool movement at high cutting speed led to the occurrence of repeated oscillations of material plastic flow and the formation of adiabatic shear

bands in chips. The spacing between shear bands was disordered at the onset of transition from continuous to discontinuous chips, but the periodic features of spacing appeared when the cutting speed increased.

These previous studies show that the discontinuous chip formation involves the oscillatory plastic flow of chip materials, and the oscillatory variation of stress, strain and temperature in time. The oscillatory phenomena in the formation process of discontinuous chips are caused by the shear localization instability. However, the continuous chip formation is related to steady plastic flow and steady evolution of stress, strain and temperature in time. Since the chip is subjected to compression-shear combined stress loading in the orthogonal cutting process, the one-dimensional cutting model established for the case of shear banding instability mainly describe the role of shear stress, but with no influence of compressive stresses on the instability mechanisms of chip materials taken into account. To clarify the problem is very helpful for thoroughly understanding the instability mechanisms of chip materials in cutting process and the nature of transition from continuous to discontinuous chips. However, the previous studies didn't pay sufficient attention on the influence of compressive stresses on the instability mechanisms. This article addresses some aspects of the problem on the bases of analysis of material instability behaviors under complex stress loading conditions.

In this study, a two-dimensional perturbation analysis of material instability under plane strain loading is first carried out and the corresponding instability criterions are established. Then, comprehensive and precise pictures of the instability phenomena in plane strain state are described by using the instable phase maps of the model material of AISI 4340 steel, which is assumed to comply with the Johnson–Cooke (J–C) constitution model. And then, the material instability behaviors and the mechanisms underlying the transition from continuous to discontinuous chips in the orthogonal cutting are studied based on the two-dimensional instability criterions. Finally, the results are discussed and summarized.

2. Basic theory

2.1. Problem formulation

Consider a general plane configuration in the x–y coordinate plane of which the thickness extends to infinite in the direction of axis z as a long column (the plane strain state) or to infinitesimal as a thin plate (the plane stress state), as shown in Fig. 1. The impact loadings in the x–y plane are assumed not to be changed in the direction of z. Thus, all components of displacements and velocities of material particles as well as the components of stresses and strains are functions of spatial coordinates x, y and time t. Our attention will focus on the instability of the plane configuration under plane loading. The governing equations include the equation of momentum balance

$$\begin{aligned}\frac{\partial \sigma_x}{\partial x}+\frac{\partial \tau_{xy}}{\partial y}&=\rho\frac{\partial^2 u_x}{\partial t^2},\\ \frac{\partial \tau_{yx}}{\partial x}+\frac{\partial \sigma_y}{\partial y}&=\rho\frac{\partial^2 u_y}{\partial t^2},\end{aligned} \tag{1}$$

the equation of energy conservation

$$\rho c\frac{\partial \theta}{\partial t}=\lambda\left(\frac{\partial^2\theta}{\partial x^2}+\frac{\partial^2\theta}{\partial y^2}\right)+\xi\left(\tau_{xy}\dot{\varepsilon}_{xy}+\sigma_x\dot{\varepsilon}_x+\sigma_y\dot{\varepsilon}_y\right) \tag{2}$$

and the equation of kinematic compatibility

$$\frac{\partial^2\varepsilon_x}{\partial y^2}+\frac{\partial^2\varepsilon_y}{\partial x^2}-\frac{\partial^2\varepsilon_{xy}}{\partial x\partial y}=0. \tag{3}$$

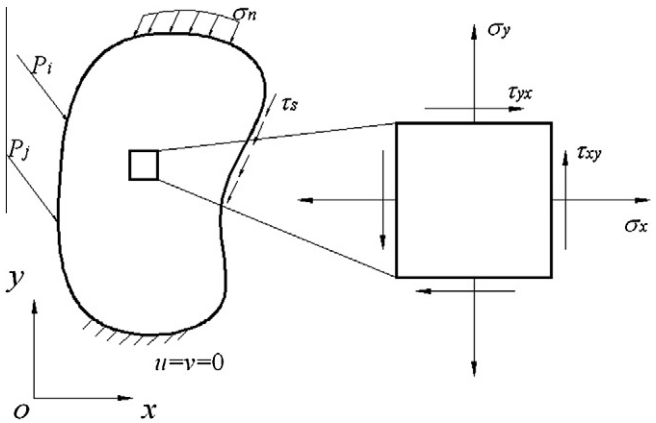

Fig. 1. The plane configuration with its loading conditions and stress state used in the present study.

In Eqs. (1)–(3), ρ is mass density. σ_x, σ_y and τ_{xy} are the components of stresses, ε_x, ε_y and ε_{xy} are the strain components, u_x and u_y are the displacement components in the direction of x and y, respectively. θ is the temperature. c, λ and ξ are respectively the volumetric specific heat, the thermal conductivity and the Taylor–Quinney coefficient which denotes the fraction of plastic work converted into heat. The dots "$\cdot$" over the quantities denote the time differential.

A simple material model used is that the material exhibits no strain rate history effects and is incompressible and isotropic. Moreover, the effect of elasticity is negligible compared with the large plastic deformation. Thus, the thermal viscoplastic behavior of material is described by the following constitutive relation in its general form

$$\sigma_{ij} = f(\varepsilon_{ij}, \dot{\varepsilon}_{ij}, \theta). \tag{4}$$

From constitutive model (4), we obtain strain hardening Q, strain-rate hardening R and thermal softening P as

$$Q = \frac{\partial \sigma_{ij}}{\partial \varepsilon_{ij}}, \quad R = \frac{\partial \sigma_{ij}}{\partial \dot{\varepsilon}_{ij}}, \quad P = -\frac{\partial \sigma_{ij}}{\partial \theta}. \tag{5}$$

Where summation is not implied for the repeated subscripts.

Localized shear instability deals with complicated constitutive behaviors of materials such as dislocation, strain gradient effect, size effect and recrystallization, and some relevant constitutive models have been proposed to describe these behaviors (see the review paper of Liang and Khan (1999)). Recently, the viscoplastic constitutive model established by Farrokh and Khan (2009) were adopted to address the size effect of grains by introducing the Hall–Petch relation into the constitutive model in addition to the hardening effects that is related to the strain and strain rate sensitivity and the thermal softening due to temperature rise. Therefore, one may attempt to use the model to describe the size effect and recrystallization occurring in the shear bands. However, our present attention is concentrated on the plastic flow behaviors of materials in the dynamic loading process. Johnson–Cook constitutive model describes the behaviors sufficiently well and deals with the effects of work hardening, strain-rate hardening and thermal softening of materials caused by impact loading. For simplicity, the J–C constitutive model is used in this work and is given by (Johnson and Cook, 1983)

$$\sigma = (A_0 + B_0\varepsilon^n)\left(1 + C_0 \ln\frac{\dot{\varepsilon}}{\dot{\varepsilon}_0}\right)\left[1 - \left(\frac{T - T_r}{T_m - T_r}\right)^m\right], \tag{6}$$

where σ and ε are the Mises effective stress and plastic strain, respectively. $\dot{\varepsilon}$ is the effective plastic strain rate, and $\dot{\varepsilon}_0$ is reference strain rate with the value 1.0 s^{-1}. T_r and T_m are the reference temperature and melting point temperature of materials, respectively. A_0 and B_0 are the initial yield stress and work hardening stress. n, C_0 and m are the coefficients of work hardening, strain-rate sensitivity and thermal softening.

High speed cutting process of materials is a typical dynamic process. Generally, the cutting speed is of the order of 10^0–10^2 m/s and the strain rate is in the range of 10^3–10^6 s^{-1}. Workpiece subjects to larger plastic strain of about 3–10 and the temperature of primary shear zone reaches the melting point of materials. Thus, work hardening, strain-rate sensitivity and thermal softening affect strongly the instability behavior of materials. From relation (5), we obtain the work hardening, strain-rate sensitivity and thermal softening corresponding to the J–C model (6) as follows:

$$\begin{cases} Q = \frac{\partial \sigma}{\partial \varepsilon} = B_0 n \varepsilon^{n-1}\left(1 + C_0 \ln\frac{\dot{\varepsilon}}{\dot{\varepsilon}_0}\right)\left[1 - \left(\frac{T-T_r}{T_m-T_r}\right)^m\right] \\ R = \frac{\partial \sigma}{\partial \dot{\varepsilon}} = (A_0 + B_0\varepsilon^n) C_0 \frac{\dot{\varepsilon}_0}{\dot{\varepsilon}}\left[1 - \left(\frac{T-T_r}{T_m-T_r}\right)^m\right] \\ P = -\frac{\partial \sigma}{\partial T} = (A_0 + B_0\varepsilon^n)\left(1 + C_0 \ln\frac{\dot{\varepsilon}}{\dot{\varepsilon}_0}\right)\frac{m}{T_m - T_r}\left(\frac{T-T_r}{T_m-T_r}\right)^{m-1} \end{cases} \tag{7}$$

In the next section, we will use J–C model (6) to describe the plastic flow of workpiece material and use the result of (7) to study the instability behaviors of chip materials caused by complex stresses in high speed cutting process.

2.2. Linear perturbation analysis

For the plane strain state, the two momentum equations in (1) can be integrated into a single equation. Thus, the system of equations governing thermal viscoplastic response of materials (1)–(3), are rewritten as

$$\begin{cases} \rho \frac{\partial^2 \varepsilon_{xy}}{\partial t^2} = \frac{\partial^2 (\sigma_x + \sigma_y)}{\partial x \partial y} + \frac{\partial^2 \tau_{xy}}{\partial x^2} + \frac{\partial^2 \tau_{xy}}{\partial y^2} \\ \rho c \frac{\partial \theta}{\partial t} = \lambda\left(\frac{\partial^2 \theta}{\partial x^2} + \frac{\partial^2 \theta}{\partial y^2}\right) + \xi(\tau_{xy}\dot{\varepsilon}_{xy} + \sigma_x \dot{\varepsilon}_x + \sigma_y \dot{\varepsilon}_y) \\ \frac{\partial^2 \varepsilon_x}{\partial y^2} + \frac{\partial^2 \varepsilon_y}{\partial x^2} - \frac{\partial^2 \varepsilon_{xy}}{\partial x \partial y} = 0 \end{cases} \tag{8}$$

Let symbol Ψ_{ij} represent stress σ_{ij}, strain ε_{ij} and temperature θ. Ψ_{ij0} is a homogeneous solution of system (8), then the stability of the homogeneous solution Ψ_{ij0} can be studied by seeking non-homogeneous solution Ψ_{ij}. To perform the linear perturbation analysis on system (8), infinitesimal perturbations on the quantities of Ψ_{ij} are introduced by

$$\Psi_{ij} = \Psi_{ij0} + \delta\Psi_{ij} \exp[\alpha_1 t + ik_1(x + y)], \tag{9}$$

where $i, j = x$ and y, $\delta\Psi_{ij}$ stands for the perturbation amplitudes which are much smaller than that of homogeneous solution Ψ_{ij0}. The wave number k_1, in the case of shear band instability, is in inverse proportion to the periodic perturbation wavelength in the direction perpendicular to shear bands. α_1 is the time growth rate of the perturbations of stresses, strain rates and temperature.

Substitution of expression (9) into system (8), and maintenance of first order terms in the perturbation increments $\delta\Psi_{ij}$ lead to a set of homogeneous equations in the form of

$$\begin{cases} \rho\alpha^2\delta\varepsilon_{xy} + k^2\delta\sigma_{xy} + \beta k^2(\delta\sigma_{kk} + \delta\sigma_{xy}) = 0 \\ \xi(\alpha\sigma_{xy0}\delta\varepsilon_{xy} + \dot{\varepsilon}_{xy0}\delta\sigma_{xy}) - \left(\alpha\rho c + \lambda k^2\right)\delta\theta - \beta\left[\lambda k^2\delta\theta - \varphi\alpha(\sigma_{x0}\delta\varepsilon_x + \sigma_{y0}\delta\varepsilon_y) - \varphi(\dot{\varepsilon}_{x0}\delta\sigma_x + \dot{\varepsilon}_{y0}\delta\sigma_y)\right] = 0 \\ \delta\varepsilon_{xy} - \delta\varepsilon_{kk} = 0 \end{cases} \tag{10}$$

where ξ is the Taylor–Quinney coefficient denoting the fraction of plastic work converted to heat with value of 0.93. If the coefficient determinant of the homogeneous system of (10) equals to zero, we obtain a characteristic equation given by, in dimensionless form,

$$\begin{aligned} &\alpha^3 + [C + (A+1)k^2]\alpha^2 + (Ak^2 + 1 - B)k^2\alpha + k^4 \\ &\quad + \beta\left\{[(2A+1)k^2 + \Pi]\alpha^2 + \left[2(1-B) + 5Ak^2 + \frac{3}{2}(\Gamma - \Sigma)\right]k^2\alpha + \frac{3}{2}\Pi k^2 + 5k^4\right\} = 0, \end{aligned} \tag{11}$$

where β is an index. When $\beta = 0$, Eq. (11) is reduced into the characteristic equation of one-dimensional simple shear case (Bai, 1982). When $\beta = 1$, it is the characteristic equation of the case of plane strain state. The dimensionless parameters used in Eq. (11) are defined as:

$$\begin{aligned} &\alpha = \frac{\lambda\alpha_1}{cQ}, \quad k^2 = \frac{\lambda^2 k_1^2}{\rho c^2 Q}, \quad A = \frac{cR}{\lambda}, \quad B = \frac{\xi P\tau_{xy0}}{\rho cQ}, \quad C = \frac{\lambda\xi P\dot{\varepsilon}_{xy0}}{\rho c^2 Q}, \\ &\Sigma = \frac{\xi P\sigma_{kk0}}{2\rho cQ}, \quad \Gamma = \frac{\xi PR\dot{\varepsilon}_{kk0}}{2\rho cQ}, \quad \Pi = \frac{\lambda\xi P\dot{\varepsilon}_{kk0}}{2\rho c^2 Q}, \end{aligned} \tag{12}$$

where $\sigma_{kk0} = \sigma_{x0} + \sigma_{y0}$ and $\varepsilon_{kk0} = \varepsilon_{x0} + \varepsilon_{y0}$.

For a given stress state and given wave number k, if the characteristic equation of (11) has real positive roots for the growth rate, $\alpha > 0$, then the perturbation may grow and the instability of materials is possible. However, its difference from the simple shear case is that the instability of materials under the plane strain loading conditions is not only in the mode of adiabatic shear localization as the shear band instability, but also in the mode of non-localized thermal softening as necking instability and others.

In the cases of long wavelengths ($k \to 0$) and short wavelengths ($k \to \infty$), it is easily found that the characteristic equation of (11) has merely trivial solution or real negative roots, implying that the plastic deformation is always steady and no instability occurs in the two extreme situations. On the other hand, the instability must occur when the real positive roots of Eq. (11) exist and reaches its maximum value α_m. In order to determine the value of k_m corresponding to the maximum value of α, on the one hand, we use the extremum condition $d\alpha_m/dk_m^2 = 0$ to obtain

$$k_m^2 = \frac{\Omega}{2\Psi}, \tag{13}$$

where

$$\begin{aligned} &\Psi = (A\alpha + 1) + 5\beta(A\alpha + 1), \\ &\Omega = (B-1)\alpha - (A+1)\alpha^2 - \beta[(2A+1)\alpha^2 - 2(B-1)\alpha + 3(\Sigma - \Gamma)\alpha + 3\Pi]. \end{aligned} \tag{14}$$

This result of (13) shows that the behaviors of wave number are strongly dependent on the normal stress intensity, strain rate sensitivity and uniformity of shear stresses distribution on the shear plane. On the other hand, the characteristic equation, (11), can be rewritten in the following form:

$$\begin{aligned} &(A\alpha + 1)k^4 + [(A+1)\alpha^2 + (1-B)\alpha]k^2 + \alpha^3 + C\alpha^2 \\ &\quad + \beta\left\{5(A\alpha + 1)k^4 + \left[(2A+1)\alpha^2 - 2(B-1)\alpha - \frac{3}{2}(\Sigma - \Gamma)\alpha + \frac{3}{2}\Pi\right]k^2 + \Pi\alpha^2\right\} = 0. \end{aligned} \tag{15}$$

The solution of Eq. (15) about variable k^2 is found to be

$$k_m^2 = \frac{\Omega \pm \sqrt{\Omega^2 - 4\Psi\Xi}}{2\Psi}, \tag{16}$$

where

$$\Xi = (\alpha + C + \beta\Pi)\alpha^2. \tag{17}$$

Comparing the peak wave numbers k_m given in (13) and (16), we can seek the maximum growth rate, α_m, from the solution of relation $\Omega^2 = 4\Psi\Xi$ for the plane strain loading condition. Thus, functions G_1 and G_2, which describe the instability behaviors of materials in the plane strain loading conditions, are obtained as

$$\begin{aligned} G_1 &= \frac{4\Psi\Xi}{\alpha^2} = 4(A\alpha_m + 1)(\alpha_m + C) + 4\beta(A\alpha_m + 1)[5(\alpha_m + C) + 6\Pi], \\ G_2 &= \frac{\Omega^2}{\alpha^2} = \{(A+1)\alpha_m - (B-1) + \beta[(2A+1)\alpha_m - 2(B-1) - 3(\Sigma - \Gamma) + 3\Pi t_c]\}^2. \end{aligned} \tag{18}$$

where a characteristic time $t_c = 1/a_m$ has been introduced.
Let $\beta = 0$ in expression (18), we obtain the functions of F_1 and F_2 corresponding to the case of one-dimensional simple shear (Bai, 1982) as:

$$\begin{aligned} F_1 &= 4(A\alpha_m + 1)(\alpha_m + C), \\ F_2 &= (A+1)^2\left(\alpha_m - \frac{B-1}{A+1}\right)^2. \end{aligned} \tag{19}$$

Like the simple shear case, the coordinates of intersections of functions G_1 and G_2 in the G-α plane determine whether the instability occurs or not. If the intersection is in the region of α>0, the instability is possible, which means

$$B + 3\beta\left[\frac{2}{3}(B-1) + \Sigma - \Gamma - \Pi t_c\right] - 2\sqrt{C + \beta(5C + 6\Pi)} > 1. \tag{20}$$

Inequality (20) gives the critical condition for estimating the instability of materials in plane strain loading conditions. By using the dimensionless parameters in expression (12) and letting $\beta = 1$, critical condition (20) is rewritten as

$$\xi P\left(2\tau_{xy0} + \sigma_{kk0} - \frac{\lambda}{c}t_c\dot{\varepsilon}_{kk0} - R\dot{\varepsilon}_{kk0}\right) - 4\left[\xi P\frac{\lambda\rho Q}{3}\left(2\dot{\varepsilon}_{xy0} + \dot{\varepsilon}_{kk0}\right)\right]^{\frac{1}{2}} > 2\rho cQ. \tag{21}$$

The critical condition of (21) indicates that, under the loading conditions of plane strain, the material instability is a very complicated phenomenon involving many influential factors, and when the thermal softening effect of plastic deformation surpasses the work hardening effect, the instability takes place. The terms inside the parentheses on the left-hand side of instability criterion (21) are dominant contribution for the thermal softening of materials and the terms within the square bracket are the secondary contribution, since, in many cases, the values of the square bracket terms are about two orders of magnitudes less than the values of the parentheses terms. We can see that the plastic flow caused by the normal stresses always enhance the thermal softening effect, and thus the plastic deformation of materials becomes further instable; however, the normal strain rate reduces the thermal softening effect and makes the plastic flow of materials tend to stable. The third term in the parentheses of criterion (21) shows the effect of heat conduction, which will stretch or shrink the plastic deformation, and the strain rate sensitivity with respect to the thermal softening of materials. Clearly, these effects induce the hardening tendency in the material plastic deformation. For a large characteristic time t_c, the heat conduction obviously extends the thermal softening zone in materials for many metals. Therefore, the occurrence probability of non-localized thermal softening instability of materials increases. However, for a small t_c, the heat conduction is not important and the thermal softening of materials in plastic deformation process tends to be localized. Thus, the instability of adiabatic shear localization takes place easily. The fourth term in the parentheses demonstrates the strain rate hardening effect related to the normal strain rates on the thermal softening of materials deformation. Similarly, the thermal softening reduction caused by the increase of normal strain rates leads to the stable trend in plastic deformation. The terms in the square bracket of critical condition (21) show that, for strain hardening material, the effects of heat conduction and strain rate hardening cause constantly the reduction of thermal softening effect of material plastic deformation. Now, we can see that the critical condition of (20) and (21) is a universal criterion for estimating the instability of materials under the plane strain loading condition. The criterion describes the instability behaviors of materials with strain hardening, strain rate sensitivity and thermal softening, with the effects of heat conduction, normal stresses and strain rates on the instability behavior taken into consideration. The mode of material instability is likely to be the adiabatic shear localization or the non-localized thermal softening.

From instability criterion (20) or (21), we can get the criteria for estimating the instability behaviors of materials under certain specific loading conditions, such as the quasi-static simple shear, tension or compression deformations and the dynamic adiabatic deformations. In the case of low strain rate loadings, such as quasi-static loading conditions, strain rate sensitivity is not important and the instability criterion of (21) is thus reduced to

$$\xi P(2\tau_{xy0} + \sigma_{kk0}) > 2\rho cQ. \tag{22}$$

The result shows that instability occurs when the thermal softening caused by the plastic work done by shear stresses and normal stresses surpasses the work hardening of materials. The instable modes of materials may be the shear localization instability or non-localized thermal softening instability caused by the plane strain loadings. If $\tau_{xy0} \gg \sigma_{kk0}$, the shear localization instability is possible; whereas for $\sigma_{kk0} \gg \tau_{xy0}$, the non-localization instability as necking occurs. Therefore, what kind of instability mode occurs depends on the ratio of plastic work done by shear stresses and that by normal stresses. If $\sigma_{kk0} = 0$ is set in Eq. (22), the criterion for instability of materials is rewritten as

$$\xi P\tau_{xy0} > \rho cQ \tag{23}$$

for one-dimensional simple shear loading condition (Bai, 1982). So this criterion does describe the shear localization instability of materials. When the thermal softening effect caused by shear stress is omitted in (22) and $\sigma_{kk0} = \sigma_x > 0$ and $\sigma_y = 0$ are set, then (22) becomes

$$\xi P\sigma_x > 2\rho cQ. \tag{24}$$

This criterion describes the non-localized thermal softening instability of materials in the necking mode under simple tension condition. If the $\sigma_x < 0$ is compressive stress, the criterion depicts the non-localization instability behavior of column sample under compressive loadings. When the effect of heat conduction is not evident as the case of high speed impact, the instability criterion of (21) takes the form of

$$\xi P\left(2\tau_{xy0} + \sigma_{kk0} - R\dot{\varepsilon}_{kk0}\right) > 2\rho cQ. \tag{25}$$

This is the instability criterion for non-heat-conducting materials under plane strain loading conditions. Clearly, under adiabatic conditions, the plastic flow of materials appear to be less stable since only the strain rate hardening cut down the thermal softening. If the effect of normal stress is small, the occurrence of instability in the mode of adiabatic shear band is possible. When the normal stress intensity is larger than that of shear stress, the shear localization instability is hardly to occur and the possibility of instability from non-localized thermal softening increases obviously. If the effects of normal stresses and strain rates are neglected, instability criterion (21) is simply reduced to the following form:

$$\xi P\tau_{xy0} - 2\left(\xi P\frac{2\lambda\rho Q\dot{\varepsilon}_{xy0}}{3}\right)^{\frac{1}{2}} > \rho cQ. \tag{26}$$

This is the criterion for the shear localization instability of materials under inhomogeneous simple shear loading. Considering the strain rate sensitivity of shear deformation, we can see that, in the case of inhomogeneous simple shear, the reduction of thermal softening effect caused by shear strain rate sensitivity is nothing but two third of thermal softening effects appearing in the homogeneous simple shear case (refer to the criterion of (32) below). Therefore, the shear localization deformation is the most instable, though the influence of the strain hardening is generally trivial at the moment.

From function G_2 in (18) and the definition of nondimensional quantity α in (12), we obtain the characteristic time of t_{c1} as

$$t_{c1} = \frac{1}{\alpha_1} \approx \frac{2\rho cR + 4\rho\lambda/3}{\xi P\left(2\tau_{xy0} + \sigma_{kk0} - R\dot{\varepsilon}_{kk0}\right) - 2\rho cQ}. \tag{27}$$

Neglecting the influences of normal stresses and strain rates on the thermal softening of materials and further considering the adiabatic shear deformation, we get the characteristic time in simple shear case (Bai, 1982) as

$$t_{c1} \approx \frac{\rho cR}{\xi P\tau_{xy0} - \rho cQ}. \tag{28}$$

A comparison of the results in (27) and (28) shows that, under the plane strain loading condition, the thermal conduction and strain rate hardening increase the characteristic time t_{c1}, and the normal stresses always reduce the time t_{c1}.

2.3. Results and discussion

In this study, AISI 4340 steel is chosen as model material since its mechanical properties and cutting mechanisms have been widely studied. The relevant data of material are easily found (Johnson and Cook, 1985). For studying the orthogonal cutting mechanisms of the steel, we first focus our attention on the instability behaviors of the steel under plane strain loading conditions. For the purpose, setting $\varepsilon = 10$, $\dot{\varepsilon} = 10^5\ \mathrm{s}^{-1}$ and $T = 10^3\ ^\circ\mathrm{C}$, and then we find the orders of the strain hardening, strain-rate hardening and thermal softening in expression (7) to be about $Q \sim 10^8$, $R \sim 10^2$ and $P \sim 10^7$. Furthermore, we estimate the orders of the dimensionless quantities in expression (12) as $A \sim 10^3$, $B \sim 10^0$, $C \sim 10^{-4}$, $\Sigma \sim 10^0$, $\Gamma \sim 10^{-1}$ and $\Pi \sim 10^{-4}$.

To study the influences of normal stresses and strain rates on instability mechanisms of materials under the plane strain loading conditions, it is necessary to compare the instability behaviors under one-dimensional simple shear state and plane strain state. Therefore, we assume that the plastic work of shear deformation in simple shear state is identical to that of plastic deformation under the plane strain loading of tension-shear or compression-shear combined stresses. That is to say, the dissipated rate of energy of plastic deformation of materials is indistinguishable under these two different loading conditions. Denote respectively the plastic work of material deformation under the one-dimensional homogeneous shear loading condition and the plane strain loading condition with $\dot{W}_1^p$ and $\dot{W}_2^p$, then

$$\dot{W}_1^p = \dot{W}_2^p, \tag{29}$$

where

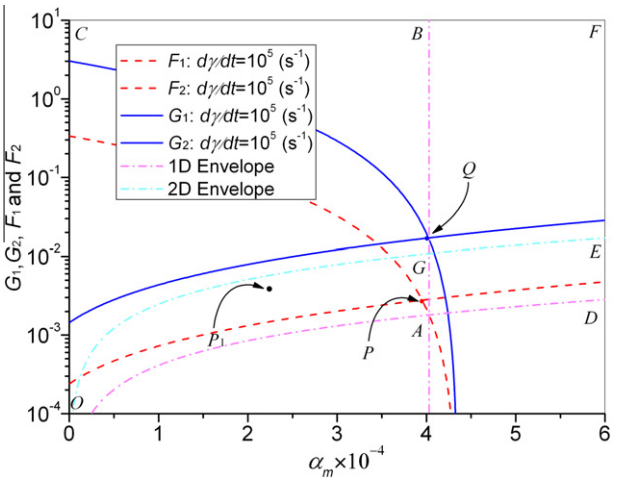

Fig. 2. The phase map illustrating the instability conditions of materials under one-dimensional simple shear and complex stress loading conditions.

$$\dot{W}_1^p = \tau_0 \dot{\varepsilon}_0, \qquad \dot{W}_2^p = \sigma_x \dot{\varepsilon}_x + \sigma_y \dot{\varepsilon}_y + \tau_{xy} \dot{\varepsilon}_{xy} \tag{30}$$

and τ_0 and ε_0 are the shear stress and shear strain in one-dimensional shear state; σ_x, σ_y, τ_{xy}, ε_x, ε_y and ε_{xy} are the components of stresses and strains in plane strain state, respectively. Thus, we can investigate the influences of normal stress and strain rates on material instability with the *phase map* for describing the material instability.

Fig. 2 is the phase map describing material stability under one-dimensional simple shear and plane strain loading states. The group of red curves in this map is obtained from the functions F_1 and F_2 in the expression (19) and thus the intersection P denotes the instability condition of materials in shear localization deformation under one-dimensional simple shear. Note that, for different strain rates, the values of F_1 and F_2 as the functions of growth rate α_m vary in the $F - \alpha_m$ plane, but the intersection P of these functions always fall in the region $OABC$ which is embraced by the boundaries CO, OA and AB. Based on the simple shear instability criterion proposed by Bai (1982)

$$B - 2\sqrt{C} > 1, \tag{31}$$

which can also be obtained by setting $\beta = 0$ in criterion (20), or rewritten as

$$\xi P \tau_{xy0} - 2\left(\xi P \lambda \rho Q \dot{\varepsilon}_{xy0}\right)^{\frac{1}{2}} > \rho c Q. \tag{32}$$

The intersection P falling in the region $OABC$ implies the occurrence of shear localization instability of materials. Therefore, strictly speaking, the intersection P stands for the critical condition of adiabatic shear localization instability of material or the condition of which adiabatic shear band fully developed under one-dimensional simple shear condition. In fact, the region $OABC$ defines the universal conditions of shear localization instability of materials under plane loading conditions. That is to say, the other points as P_1 in the region correspond to the instability conditions of adiabatic shear localization under the complex stress states. Whereas, outside the region $OABC$, the material instability, if happening, will not be in the adiabatic shear localization, perhaps in non-localized thermal softening instability such as necking under simple tension loading condition or the steady plastic flow. Note that the position of the boundary AB of region $OABC$ is determined by the horizontal coordinate of intersection A of function F_2 curve with the envelope OAD, and thus depends on shear strain rates. In this figure, the boundary AB corresponds to strain rate 10^5 s^{-1}. When the strain rate increases, the boundary shifts in the positive direction of α_m axis; while the strain rate decreases, the boundary moves in the negative direction of α_m axis. Thus, the region $OABC$ varies with the loading rates evidently.

The group of blue[1] curves in Fig. 2 is obtained from the functions G_1 and G_2 in (18). The intersection Q of G_1 and G_2 shows the critical conditions of material instability in the shear localization deformation if Q is inside the region $OABC$, or shows the critical condition of non-localized thermal softening instability or the steady plastic flow if Q is inside the region $GEFB$. Note that the point Q here denotes the shear localization instability condition under inhomogeneous simple shear loading condition which corresponds to the critical condition (26). Similarly, we found that the curves of function G_2 are constantly above a bottom boundary OGE for various loading rates. The point Q inside the region $OEFC$ denotes the general instability conditions of materials under complex stress loading conditions which include the cases of simple tension or compression loadings. Therefore, in region $OEFC$, the instability criterion of (20) and (21) describes the general instability conditions of

[1] For interpretation of color in Figs. 2–5, 7, 10–12, the reader is referred to the web version of this article.

materials as the shear localization deformation, non-localized thermal softening and the steady plastic flow. Unlike region *OABC*, region *OEFC* is open on the right-hand side. Thus, the right boundary *AB* of region *OABC* divides the region *OEFC* into two parts. The possible instability conditions of adiabatic shear localization under combined stress loading states are applied to region *OGBC* locating inside the region of *OABC*. The instability conditions of non-localized thermal softening under combined stress loading states are applied to region *GEFB* outside the region *OABC*. As for the remaining regions in the phase map, such as the region below the boundary *OAD* and the region with $\alpha_m < 0$, the plastic deformation is always stable under complex stress loading conditions. Note that boundary *OGE* of region *OEFC* is always above boundary *OAD*, which shows that the area of region *OGBC* is constantly less than the area of the region *OABC*. Therefore, the shear localization instability under combined stress loading conditions is relatively difficult to occur compared with the one-dimension homogeneous shear loading condition. This is because that the energy dissipated by shear localization deformation in the case of combined stress loading conditions is less than that in the case of homogeneous simple shear condition. When the loading effects of complex stresses disappear, boundary *OGE* is found to approach boundary *OAD*.

A comparison of critical condition (26) with one-dimensional simple shear instability criterion (32) shows that the inhomogeneities of shear stresses and temperatures distributing on shear plane enhances the probability of shear localization instability to some degree due to the increase of thermal softening effect. By comparing the horizontal coordinates between the points *P* and *Q* in Fig. 2, we can see that the horizontal coordinate α_m at point *Q* is slightly larger than that at point *P*, implying that the shear localization deformation in the inhomogeneous shear case is relatively unstable. The increase of thermal softening effect of plastic deformation is principally caused by the inhomogeneities of shear stress and temperature distributing on the shear plane. The small difference of horizontal coordinate α_m denotes that both the thermal softening effect and the characteristic time required of material instability are almost identical in the cases of homogeneous shear and inhomogeneous shear.

Owing to various loading modes of complex stresses, the plastic deformation of materials exhibits complex instability behaviors. In the following text, we will concentrate on the instability behaviors of materials for three different complex stress loading conditions.

2.3.1. Case 1. Invariable strain rates and variable stresses

Suppose that the plane configuration in Fig. 1 is subjected to such dynamic loading conditions of plane strain state that the shear and normal strain rates have the same order of $10^5\ s^{-1}$, and the intensities of shear stress decrease from 0.2 GPa to zero, while the intensities of normal stresses increase from zero to 0.2 GPa. These situations correspond to the transition from the dynamic shear loading state with an initial static normal stresses to the dynamic tension or compressive loading state with an initial static shear stresses. Based on the energy balance principle, that is, the reduction of plastic work induced by the decrease of shear stress should equal to the enhancement of plastic work caused by the increase of normal stress, we can study the effects of normal stresses on the instability, with its phase map shown in Fig. 3.

The phase map in Fig. 3a demonstrates the material instability conditions in the case of tension-shear combined stress loadings, where points *P* and *Q* denote, similar to those used in Fig. 2, the instability conditions of shear localization deformation in the homogeneous and inhomogeneous shear loading cases, respectively. When the magnitude of shear stresses is reduced and the magnitude of tensional stresses is enhanced, the intersections Q_i of functions G_1 and G_2 shift in the negative direction of α_m axis on the curve of function G_1 as shown by point Q_2. Obviously, the material instability in the shear localization deformation denoted by point Q_2 becomes relatively difficult to occur since the perturbation growth rate α_m is

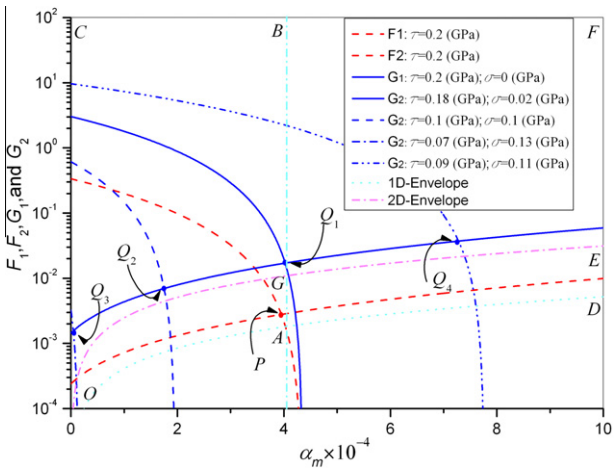

Fig. 3a. The phase map of material instability for the loading conditions of tension-shear combined stresses, in which varied tension stresses and constant strain rates are assumed.

considerably reduced. In physical sense, the increase of tensional stress in magnitude strengthens the non-localized thermal softening effect of materials and the decrease of shear stress in magnitude weakens the localization thermal softening effect.

When the magnitude of shear stress reduces continuously, intersections Q_i of G_1 and G_2 approach the left boundary, OC, of region $OABC$ and finally gets into the region with $\alpha_m < 0$, which implies that the plastic deformation of materials under the tension-shear combined stress loading conditions is constantly stable. From expressions (12) and (27), we can see that, when $\alpha_m \to 0$, the characteristic time, t_c, increases sharply; accordingly, the term Πt_c in function G_2 is greatly enhanced. The non-dimensional parameter Π with the order of 10^{-4} denotes the effects of the thermal softening and strain hardening related to normal strain rate sensitivity on instability. When α_m varies around the order of 10^{-4}, the influence of Πt_c on the instability is not obvious; however, when $\alpha_m < 10^{-4}$, then $t_c > 10^4$, the role of Πt_c becomes evident. From expressions (12), the relation between t_c and t_{c1} is found to be $t_c = cQt_{c1}$ and the proportionality coefficient, cQ, is of the order of 10^{10}. When $t_c > 10^7$, $t_{c1} > 10^{-3}$ s, which means that the instability in shear localization deformation caused by the tension-shear combined stresses, if occur, is a relatively slow dynamic process with low impact speeds. For the plastic deformation with large characteristic time t_{c1}, the heat conduction effect often yields strong non-localized thermal softening in materials and weakens the work hardening evidently. If the work hardening is still the dominant influence factor for the plastic deformation, intersection Q_i of functions G_1 and G_2 will get into the region with $\alpha_m < 0$ and the plastic deformation is stable. However, the reduction of growth rate α_m would result in a great increases of characteristic time t_c, or the term Πt_c in orders. When the loading rate is low, the strain softening ($Q < 0$) of materials often occurs and becomes dominative factor for the instability of materials. At the moment, the term Πt_c in function G_2 changes its sign from plus to minus, and point Q_i shifts inversely in the positive direction of α_m axis and rapidly gets into the region right to boundary AB, as shown by point Q_4 in Fig. 3a. The point Q_4 in the region of $GEFB$ denotes the initial conditions of non-localization instability of materials or the long range homogeneous plastic flow. Therefore, under the tension-shear combined stress loading conditions, if the tension stress intensity is large enough and the shear stress intensity is small enough, the material instability is usually controlled by the tension stresses, and the instability occurs in the non-localized thermal softening deformation. Such a typical example can be easily found. Let $\sigma_y = 0$ when $|\tau_{xy}| \to 0$, and keep $\sigma_x = Const$, the loading condition closes to the condition of simple tension loading. Then, the material instability in necking model occurs. Point Q_3 in this figure denotes the critical condition at which the instability of materials in the shear localization transits to the instability in the non-localized thermal softening or into homogeneous plastic flow of material deformation. It is found that the ratio of plastic work of shear deformation and that of stretching deformation at point Q_3 is about 1:2. Therefore, under the loading condition of tension-shear combined stresses, when the plastic work dissipated by tension deformation reaches 67% of the total, the instability behaviors of material plastic flow change from the shear localization deformation to the stable plastic flow, if strain hardening prevails ($Q > 0$); otherwise, the instability mode of materials transits from the shear localization instability to the non-localized thermal softening instability or get into long range homogeneous plastic flow if thermal softening occur ($Q < 0$).

Fig. 3b shows the phase map of material instability under the loading conditions of compression-shear combined stresses. We can see that, when the magnitude of shear stresses decreases and the magnitude of compressive stresses increases, the instability of materials in the shear localization deformation becomes relatively difficult to occur compared with the inhomogeneous shear situation Q_1 since the α_m value of point Q_2 is less than that of point Q_1. Similar to the case of tension-shear combined stress, as $\alpha_m \to 0$, if there is no strain softening ($Q > 0$), the shear localization instability is quite difficult to occur due to the decreases of growth rate ($\alpha_m > 0$), or even no shear banding instability would occur if $\alpha_m < 0$. However, once the strain softening occurs ($Q < 0$), the strain rate sensitivity affects strongly the instability behavior and intersection Q_i of functions G_1 and G_2 turns backward to shift into the region right to boundary AB, as shown by point Q_4. Therefore, intersection Q_4

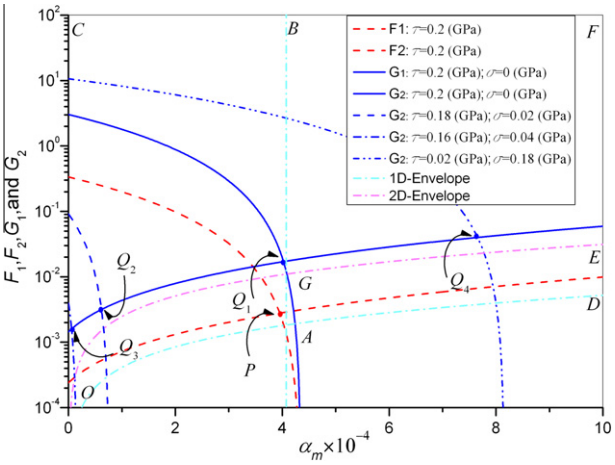

Fig. 3b. The phase map of material instability for the loading conditions of compression-shear combined stresses, in which varied compression stresses and constant strain rates are assumed.

indicates that material undergoes either the non-localized thermal softening instability or the homogeneous plastic flow under the compressive-shear stress combined stresses. A typical example of such instability is the catastrophic failure of metallic column samples under uniaxial compressive loading conditions. Also, point Q_3 denotes the critical condition at which the instability mode transits from the shear localization deformation into the non-localized thermal softening or the homogeneous plastic flow. The ratio of plastic work of the shear and that of the compressive deformation is about 39:11, implying that, when the plastic work dissipated by compressive deformation reaches about 20% of the total, the transition of material instability modes occurs.

By comparing the critical conditions at point Q_3 in Figs. 3a and 3b, we can see that, in compression-shear combined stress loading state, when the intensity of compressive stress is about 25% of the shear stress intensity, the instability mode of materials changes from the shear localization instability to the non-localized thermal softening instability or the homogeneous plastic flow. However, in the tension-shear combined stress state, when the tension stress intensity is twice as large as the shear stress intensity, the transition of instability modes takes place. This result shows that, under the combined stress loading conditions, the shear localization instability of materials is much more sensitive to the compressive stress than to the tension stress.

2.3.2. Case 2. Invariable stresses and variable strain rates

To study the effects of different strain rate on the instability behaviors, consider the case of constant stresses and variable strain rates. Now we focus our attention on two specific cases in which the ratios of tension or compression stress and shear stress are initially prescribed. The shear stress intensity in the combined stress state is assumed to be the same as that in the homogeneous simple shear state. Thus, the localization thermal softening caused by shear stresses is identical in the two cases and in the initial state, the instability of shear localization deformation always occurs. Therefore, points Q_i denoting the instability conditions are inside the shear localization instability region, *OABC* (Fig. 4).

The phase map in Fig. 4a shows the instability conditions for the case with different strain rates and constant tension-shear combined stresses. Point P denotes the shear localization instability condition under simple shear loading. Point Q_1 indicates the shear localization instability condition in which the plastic work of shear deformation equals the plastic work of stretching deformation in tension-shear combined stress loading conditions, that is, the intensities of both tension stress and shear stress are assumed to be 0.2 GPa and the tension and shear strain rates are $10^5\ s^{-1}$. When the shear strain rates increase from $10^5\ s^{-1}$ to $1.5\times10^5\ s^{-1}$ and $2\times10^5\ s^{-1}$ and the related tension strain rate decreases from $10^5\ s^{-1}$ to $0.5\times10^5\ s^{-1}$ and $0\ s^{-1}$, the intersection, Q_i, of functions G_1 and G_2 change from point Q_1 to points Q_2 and Q_3 and the corresponding growth rates increase evidently. The increase of shear strain rates and the decrease of tension strain rates further reinforce the thermal softening effect caused by shear localization deformation. Hence, the shear localization instability of materials becomes easier. Contrarily, when the shear strain rates decrease from $10^5\ s^{-1}$ to $0\ s^{-1}$ and the tension strain rate increases from $10^5\ s^{-1}$ to $2\times10^5\ s^{-1}$, intersection Q_i of functions G_1 and G_2 transits from point Q_1 to Q_4 and the growth rate decreases. Hence, the instability of shear localization deformation becomes relatively difficult to occur since the localization thermal softening effect induced by shear stresses is reduced and the non-localized thermal softening effect caused by tension stresses is enhanced. However, the shear localization instability always occurs because all of the intersections, Q_i, denoting the instability conditions fall in the shear banding instability region *OABC*. Notice that, the point Q_3 corresponds to the instability condition with the shear strain rate $2\times10^5\ s^{-1}$ and free normal strain rate; thus, point Q_3 describes physically the dynamic

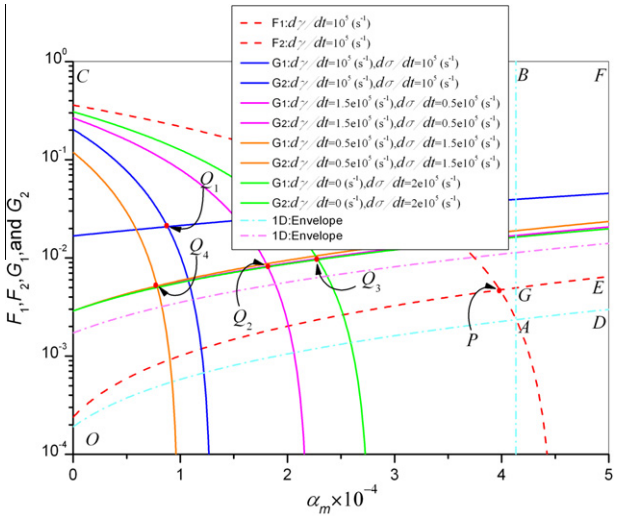

Fig. 4a. The material instability conditions illustrated by the phase map of tension-shear combined stresses, in which varied strain rates and constant tension stresses are assumed.

shear loading state with initial static tensional stresses. Similarly, point Q_4 with a shear strain rate of 0 s^{-1} and a normal strain rate of 2×10^5 s^{-1} describes the dynamic tension loading state with an initial static shear stress. Consequently, if the shear stress intensity is large enough, the shear localization instability of materials always occurs, independent of the strain rate variation.

The phase map in Fig. 4b illustrates the instability conditions of materials when the strain rates vary and the compressive stresses keep unchanged. Clearly, the influence of compressive stresses on the instability of shear localization deformation is different from that of tension stresses (Fig. 4a). Point Q_1 denotes the instability condition of shear localization deformation with the loading conditions: the intensity of compressive stresses is 0.02 GPa and the intensity of shear stresses is 0.18 GPa. Both normal and shear strain rates are 10^5 s^{-1}. Note that, for the time being, the ratio of plastic work of the shear deformation and that of the compressive deformation is 9:1. We consider a case in which the plastic work of shear deformation differs from that of compressive deformation because no shear localization instability occurs when the plastic work of compressive deformation is larger than 20% of the total.

When the shear strain rate increases from 10^5 s^{-1} to 1.11×10^5 s^{-1}, that is, the shear deformation dissipates all of the plastic deformation work, the shear localization instability denoted by point Q_2 occurs more easily compared with the initial shear banding instability condition of Q_1. When the shear strain rate has a small reduction, such as from 10^5 s^{-1} to 0.9×10^5 s^{-1}; that is, the plastic work dissipated by shear deformation is above 80% of the total, the shear banding instability of materials denoted by point Q_3 is still possible. When the shear strain rate reduces from 10^5 s^{-1} to 0.5×10^5 s^{-1} and then the plastic work of compressive deformation is about 55% of the total, the plastic flow state of materials is at a turning point. Corresponding critical condition for the instability of materials is denoted by point Q_4 on boundary *AB*. Therefore, if the plastic work of compressive deformation is less than 55% of the total, the shear localization instability would occur; otherwise, the non-localized thermal softening instability caused by compressive-shear combined stresses takes place. When the shear strain rate approaches to zero and the compressive strain rate is 10^6 s^{-1}, the compressive deformation dissipates total plastic work power, and thus the shear banding instability is absolutely not possible. The instability of non-localized thermal softening caused by compressive stresses shown by point Q_5 always occurs, and the instability behavior is affected by the loading conditions of dynamic compression stresses with initial static shear stress.

Now, we can see that, for different combined stresses loading conditions, the influences of strain rates on material instability behaviors are quite different. In the case of tension-shear combined stress loading, the shear localization instability is always possible when the shear strain rates change in the region from 0 to 10^5 s^{-1}, that is, as long as the shear stress intensity is strong enough, the shear localization deformation always occurs no matter the loading conditions are the combination of dynamic tension and static shear or that of dynamic shear and static tension. However, under the loading conditions of compression-shear combined stresses, both shear localization instability and non-localized thermal softening instability are possible when the shear strain rates vary, and what kind of instability will occur depends on the ratio of plastic work of compressive deformation and that of shear deformation.

2.3.3. Case 3. Variable strain rates and stresses

Generally, the stresses and strain rates applied on material element (Fig. 1) are variable simultaneously; hence, it is necessary to consider the influences of variable stresses and variable strain rates on the instability behaviors of materials. The phase maps in Fig. 5 illustrate the instability conditions of materials when the stresses and strain rates are all changed. When the plastic work of stretching deformation increases from 0 to 20 $GPas^{-1}$ (Fig. 5a), intersection Q_i of functions G_1 and G_2

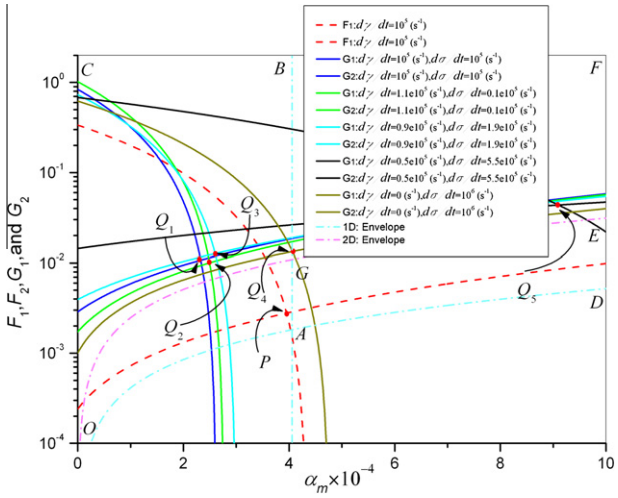

Fig. 4b. The material instability conditions illustrated by the phase map of compression-shear combined stresses, in which varied strain rates and constant compression stresses are assumed.

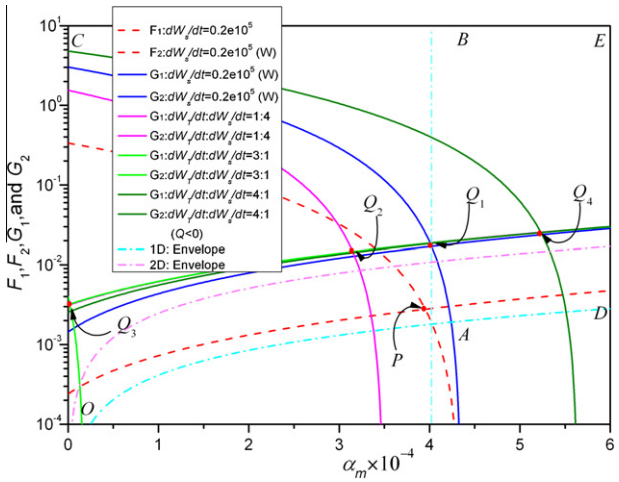

Fig. 5a. The material instability conditions illustrated by the phase map of tension-shear combined stresses, in which both the strain rates and the tension stresses are assumed to be varied.

denoting the instability conditions moves from Q_1 to Q_2, implying that the shear localization instability of materials becomes relatively difficult to occur. When the plastic work of stretching deformation increases to about 75% of the total, corresponding intersection Q_3 reaches the boundary OC and the shear localization instability of materials is not possible. When the plastic work of stretching deformation accounts for 75% or more of the total, the plastic flow is always stable if the work softening does not occur. However, once the work softening caused by stretching deformation occurs, non-localized thermal softening instability or long range homogeneous plastic flow is possible as illustrated by point Q_4. Similarly, with the increase of the plastic work of shrinking deformation (Fig. 5b), the shear localization instability becomes difficult to occur and when the plastic work of shrinking deformation is larger than about 20% of the total, the deformation becomes stable. Only when the work softening takes place, the instability mode of non-localized thermal softening deformation or long range homogeneous plastic flow takes place.

From the analysis above on the instability behaviors of viscoplastic materials, we can see that the shear localization instability of materials is closely related to the mode of complex stress loading. In particular, it is more sensitive to the compression stress than to the tension stress. The analytical results about the sensitivity of shear localization instability to compressive stress are in agreement with the experimental observations of Walker and Shaw (1969) and Shaw (1984). In the tests of metalic specimens under compression-shear combined stresses, they found that strain softening sets in when the compressive stress is about 10% of the maximum shear stress. Shear localization instability is very difficult to occur when the compression stress increases. Moreover, Anand et al. (1987) have also studied the instability behaviors of pressure-sensitive materials. For strain softening materials, they found that slight pressure sensitivity accelerates the shear

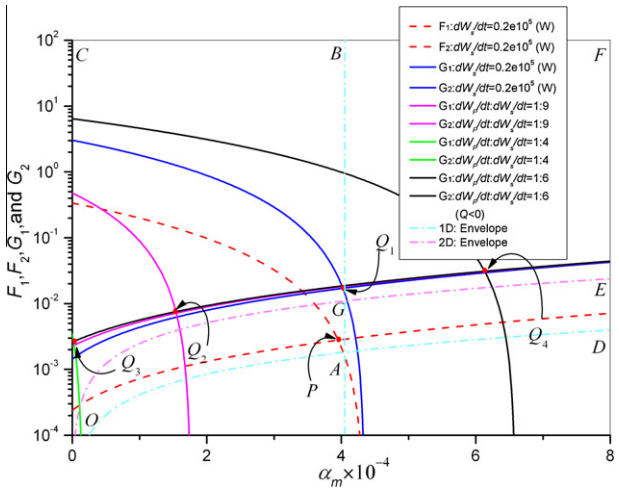

Fig. 5b. The material instability conditions illustrated by the phase map of compression-shear combined stresses, in which both the strain rates and the compression stresses are assumed to be varied.

localization instability of materials, and for strain rate hardening materials, the shear localization instability occurs when pressure hardening effect is sufficiently large.

3. Instability behaviors in orthogonal cutting process

3.1. Orthogonal cutting model

Because the shape of chips reflects, to a large degree, the removal mechanisms of chip materials from workpiece surface in machining process, it is necessary to develop a model by which we can study the formation mechanisms of chips and predict the transition from the continuous to the segmented chips based on the principle of impact dynamics. Therefore, the aim of this section is to use a two-dimensional continuum model for studying the formation and mode-transition of chips in orthogonal cutting. This is illustrated in the following discussion and extension of the present theories to the cutting process.

Fig. 6 illustrates a two-dimensional continuum model for orthogonal machining. The cutting conditions are specified by rake angle α, uncut chip thickness t, cutting speed V_c, width W and length L of the workpiece, respectively. The workpiece is moving forward to the cutting tool at a cutting speed of V_c. At present, we develop a two-dimensional model of orthogonal cutting by modified the conventional one-dimensional models (Burns and Davies, 2002) for studying the influences of normal stresses on the instability behaviors of chip materials. During the orthogonal cutting process, the material in extensive zone *DEFGHI* including the primary and secondary shear zones is assumed subjected to intensive transient stress and large plastic deformation. Hence, our attention is focused on the stress state, plastic deformation, strain rate sensitivity and thermal softening effect of materials in the *DEFGHI* zone. In this model, the shear angle of φ is not a previously prescribed constant, but is determined by numerical simulation. In what follows, the shear angle is defined as the angle between the cutting line *OE* on the new surface of workpiece and the curve *DG* on which the maximum shear strain presents. The primary shear zone is again not a prescribed narrow thin layer, as in the conventional one-dimensional model, even though quite high strain rate and large plastic deformation take place in this zone, leading to the generation of a great amount of heat. Most of the heat converted from plastic work induces a temperature rise of chip materials, and a proportion of heat is dissipated by heat conduction into the uncut workpiece material in the *DEFGHI* zone since the strain rates may be very small in the cases of low speed cutting process. The heat in the orthogonal cutting comes from two sources: one is the large plastic deformation of material occurring in the *DEFGHI* zone and another is the friction between the tool and chip influencing the material temperature rise of the secondary shear zone. For convenience, assume that 90% of the plastic deformation work is converted into heat which is conducted according to the two-dimensional governing equation, Eq. (2), for the temperature field. Now some of heat generated from the plastic deformation is assumed to be conducted into the part of uncut workpiece material and remains to be taken away by the convection of the moving chip from removed material in the primary shear zone.

Large plastic deformation of workpiece and chip during the cutting process is accompanied by heat generation and transfer, as well as by mechanical dissipation. Effects of high temperature and high strain rate on material behavior must be

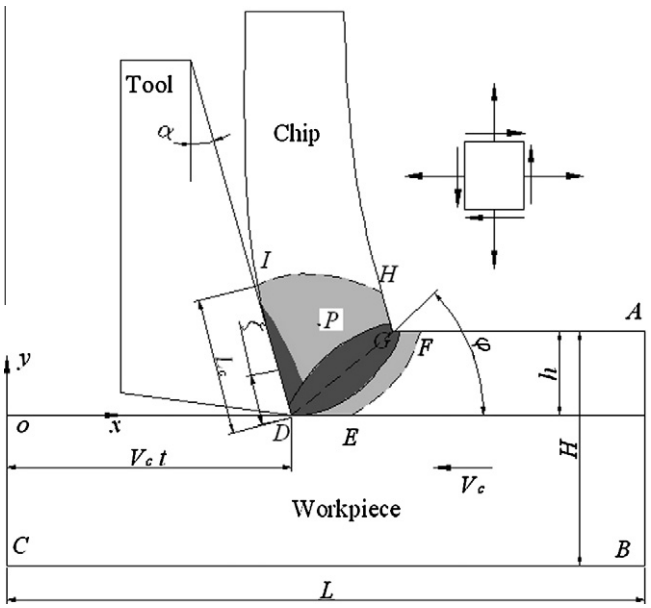

Fig. 6. Schematic of two-dimensional orthogonal cutting model used in this study.

considered when simulating the chip formation, especially in modeling plastic flow localization of materials in segmented chips. The cutting process is related to strain-rate and temperature, so material behavior is thermal viscoplastic. Assuming that (i) the workpiece material is isotropic and incompressive, (ii) elastic deformation is negligible compared with large plastic deformation of chips, (iii) the tool is treated as a rigid body and (iv) the plastic flow of material complies with von Mises yield criterion. Thus, the J–C constitutive model (6) can describe the thermal viscoplastic behavior of workpiece material. Strain hardening, strain rate sensitivity and thermal softening effects of materials are in expression (7).

In the orthogonal cutting process, forces for removing chip material from the workpiece are the forces that interact between tool tip and uncut materials. On the primary shear zone, the forces between uncut workpiece material and the chip are the resistances against the removal of chip materials. If relative movement between tool face and chip in the secondary shear zone is considered, forces removing chip material also include intense friction and compressive stresses. The frictional interaction is described by Coulomb law

$$F_c = \mu F_n, \tag{29}$$

where F_c is friction force, F_n is compressive force and μ is friction coefficient between tool face and workpiece and has the value 0.1. Furthermore, local temperature rise in the secondary shear zone is determined by heat generated through friction along the tool-chip interface. It is assumed that all frictional work is converted into heat that 90% of the heat generated will go into the chip, and that material properties do not relate to temperature. Thermal convection between workpiece and air is insignificant compared to heat generated by plastic work, but friction and thermal conduction in workpiece material must be considered.

The boundary conditions for the chip-workpiece-tool system in the orthogonal cutting process (Fig. 6) are determined as follows. The tool moves towards the right with constant cutting speed V_c while being restrained vertically. The two ends of the uncut part of the workpiece are restrained horizontally in the cutting direction but not restrained vertically. The bottom boundary of the workpiece deforms slightly during cutting and zero displacement conditions are assigned for both directions. For the orthogonal cutting process, the stress and displacement boundary conditions are

$$\begin{aligned}
&\begin{cases} y = V_c t + x\mathrm{ctg}\alpha, \\ V_c t - L_c \sin\alpha < x < V_c t \end{cases} : && \begin{cases} \sigma_n = \sigma_T, \sigma_s = \mu\sigma_T, \\ u_x = V_c t - \varsigma \sin\alpha \end{cases} \\
& && \varsigma = [(V_c t - x)^2 + y^2]^{\frac{1}{2}} \\
&x = 0, -(H-h) < y < 0 : && u_x = 0 \\
&x = L, -(H-h) < y < h : && u_x = 0 \\
&0 < x < L, y = -(H-h) : && u_x = 0, u_y = 0 \\
&0 < x < L, y = h : && \sigma_y = 0, \tau_{xy} = 0,
\end{aligned} \tag{30}$$

where σ_T is contact compressive stress on the tool face that is in contact with the chip. The first condition of (30) describes stress and displacement continuity conditions on the tool-chip interface. Metal cutting is a transient process, so adiabatic boundary conditions are used in this simulation. Temperature boundary conditions are

$$\begin{aligned}
&\begin{cases} y = V_c t + x\mathrm{ctg}\alpha, \\ V_c t - L_c \sin\alpha < x < V_c t \end{cases} : && k_h \tfrac{\partial T}{\partial x} + k_T \tfrac{\partial T_T}{\partial x} = 0 \\
&x = 0, -(H-h) < y < 0 : && \tfrac{\partial T}{\partial x} = 0 \\
&x = L, -(H-h) < y < h : && \tfrac{\partial T}{\partial x} = 0 \\
&0 < x < L, y = -(H-h) : && \tfrac{\partial T}{\partial y} = 0 \\
&0 < x < L, y = h : && \tfrac{\partial T}{\partial y} = 0,
\end{aligned} \tag{31}$$

where k_h is thermal conductivity of the workpiece, k_T is thermal conductivity of the cutting tool and T_T is tool temperature. The first equation of Eq. (31) describes heat conduction between chip and tool.

Governing Eqs. (1)–(3) and prescribed conditions of (30) and (31) are solved numerically and study of instability behaviors of AISI 4340 steel during high speed cutting process are based on instability criterion under plane strain loading conditions. Plastic work is almost completely converted into heat, so there is thermal deformation and effect on material properties and the modeling of high speed cutting requires a coupled thermo-mechanical analysis. For each time step, the heat conduction and stress analyses are performed simultaneously. The quadrilateral element of 4-node bilinear displacement and temperature, hybrid with constant pressure (CPE4HT) is used for the discretization of both the workpiece and the tool materials. Strains and deformation of elements are continuous over element boundaries (Sorenson, 1996). Fig. 7 shows finite element model of the orthogonal cutting process. To resolve large strain gradients, a high mesh density is established in the regions of strong plastic deformations along the cutting line of the workpiece. Compared with simulation results of standard elements, the difference in results of metal cutting simulation using quadrilateral elements is controlled to within 1% for local quantities like plastic deformation, Mises stress, shear strains and pressure. There is almost no effect on global quantities like cutting forces (Bäker et al., 2002).

The metal cutting process produces continuous and segmented chips. In numerical modeling of chip formation, simulation results strongly depend on the choice of element size and orientation. Formation of segmented chips is closely related to

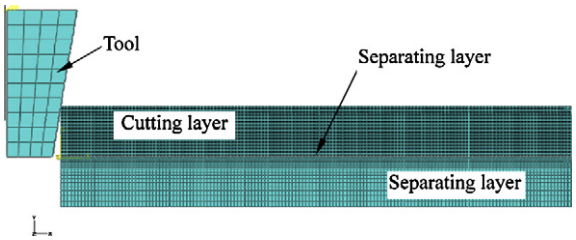

Fig. 7. The finite element model used in the modeling of metal orthogonal cutting process.

material flow localization caused by shear concentration, which may lead to finite element mesh that is too distorted to ensure solution stability and numerical convergence. Previous studies (Hortig and Svendsen, 2007; Özel and Altan, 2000) show that element natures such as orientation, edge length ratio and interpolation order significantly influence material flow localization behaviors in the modeling of adiabatic shear banding. However, the present study is designed to simulate the formation of segmented and continuous chips during the orthogonal cutting process. The choice of properties of quadrilateral elements is not designed particularly to consider the plastic flow localization that occurs in segmented chips. The desire provides a logical prediction of chip geometry, Mises stress field, shear stress and strain fields and temperature distribution in both chips and workpiece and obtains simulation results that agrees with experimental results (Komanduri, 1982).

In simulating the metal cutting process, a crucial technical problem is accurate modeling of material separation in the removed process of chip materials from the workpiece surface. Usually, a predefine separation line divides the chip and uncut workpiece materials (Fig. 7). When a certain criterion is reached, the pair of bonded nodes that lie just ahead of the tool tip on this line is released. The result is removed of chip material from the workpiece surface. The criterion for chip removed may be maximum stress criterion or equivalent plastic strain criterion or the critical damage criterion. In the present simulation, separation between the chip and the workpiece is determined by the equivalent plastic strain criterion. Generally, the value of equivalent plastic strain varies for different workpiece materials and different cutting conditions. Xie et al. (1998) show that different values may affect stress distribution and plastic deformation in a machined surface and that these values do not appear to affect chip geometry and stress distribution in chips. Therefore, from the consideration of experience, it is possible to assign a critical value of equivalent plastic strain. Here, critical equivalent plastic strain has the value 2 as Hortig and Svendsen (2007). When equivalent plastic strain is less than 2, material behaviors on the separation line follow the J–C constitutive model and equals 2, separation of materials on the line occurs.

The commercial FEM software package + helps in numerical simulation of machining process of materials because of outstanding features such as efficient modeling of the complicated contact conditions at chip-tool interfaces, convenient revelation of plastic flow and localization instability behaviors of chip materials, accurate description of removed behaviors of chips from workpiece surface and reasonable explanation of chip formation mechanisms and transition from continuous chip to segmented chip. The present simulation of cutting process is based on the dynamic analysis of ABAQUS/Explicit. Governing equations of the system are integrated using the numerical schemes of the explicit central-difference integration rule (Sorenson, 1996). To ensure the solution convergence, some special functions of the software are sued in the explicit dynamic analysis of simulating the cutting process. Initially, a stability limit is defined in terms of the highest frequency of the system ω_m as

$$\Delta t_s \leq \frac{2}{\omega_m} \tag{32}$$

Based on the smallest propagation time of dilatational wave across the minimum length of elements in the mesh, the stability limit is approximated

$$\Delta t_a \leq \frac{L_{\min}}{c_d}, \tag{33}$$

where $L_{\min}$ is the smallest element dimension in the mesh and c_d is dilatational wave speed. Stability limit may vary with automatic or fixed time incrementation parameters. To enhance solution stability, the stable time increment is adjusted with a scaling factor by specifying explicit time integration with the default global time estimation. In general, the actual stable time increment chosen by ABAQUS/Explicit is less than the estimation by a factor of between $1/2^{0.5}$ and 1 in a two-dimensional model. Thus, time increment is less than the stability limit of the central-difference operator that is used in the numerical analysis. Using a time increment that is brief enough ensures numerical stability of the algorithm and solution convergence.

3.2. Simulation and discussion

In a series of cutting experiments of AISI 4340 steel, Komanduri (1982) observed that the chip shape changed from discontinuous to continuous and then to segments. When the cutting speed falls in the region from 0.5 to 1 m/s, the chips are of continuous shape; below 0.5 m/s discontinuous chips take place; but at the cutting speeds above 2 m/s, different types of

cyclic chip morphology which lead to the catastrophic shear banding instability of material are observed. Presently, a two-dimensional numerical simulation on the cutting process of steel are performed for the purposes of repeating Komanduri's experimental observations. Moreover, it is expected to use the simulation results to estimate the instability behaviors of removed materials, the formation and transition between the continuous and discontinuous chips in high speed cutting process based on the instability criteria proposed in the previous section for complex stresses state. The material properties and parameters of model material AISI 4340 steel used in the calculation are given in Table 1.

In Fig. 8 we show the contours of Mises effective stresses, shear stress, shear strain and temperature when the cutting distance is 0.7 mm. The three groups of results obtained correspond to three cutting speeds of 0.5 m/s, 1 m/s and 1.5 m/s, respectively. It can be seen that the continuous chips of AISI 4340 steel does form as observed in Komanduri's experiments (1982).

The Mises effective stresses shown in Fig. 8a distribute in the extensive zone *DEFGHI* (Fig. 6) which is different from the situation of convention one-dimensional model (Shet, 2000; Bäker et al., 2002). The effective stresses with high intensity appear in two sizable regions: one is near the chip free surface of primary shear zone and another is at the top of secondary shear zone. When the cutting speed increases, the distributing zone in the chip more evidently separates into the primary and secondary shear zones and the peak intensity of effective stress decreases from 1.42 GPa to 1.35 GPa. A comparison of the contour plots between the effective stresses and the shear stresses (Fig. 8b) indicates that the effective stresses in the secondary shear zones is mainly the compressive stresses produced by tool and the shear stresses occur in a large region which embraces the primary shear zone and extends into the uncut workpiece materials. Note that, as the cutting speed increases, the region decreases in size. The peak intensity of shear stress decreases from 0.76 GPa to 0.73 GPa, and the peak intensity of shear stress in the region of uncut workpiece material below the primary shear region increases from 0.35 GPa to 0.45 GPa. Therefore, the general distribution tendency of the shear stresses in workpiece materials is localization and uniformity as the cutting speed increases. The shear strain contours in Fig. 8c show evidently that the plastic deformation of chip materials is nearly uniform in an extensive plastic flow region and the average shear strain reaches the orders of 3–4. The non-localization plastic deformation of chip materials indicates that the chip formation undergoes a long range steady plastic flow process under the action of tool compression, and thus, no instability of adiabatic shear localization in chip materials is observed. Fig. 8d shows the temperature contours corresponding to the three cutting speeds. We can see that the peak temperatures in chip materials increase from 418 K to 523 K as the cutting speed increases. The heat affecting zone of high temperature is inside the extensive region *DEFGHI*. The temperature rise is caused by plastic deformation

Table 1
Physical and mechanical properties of AISI 4340 steel (Johnson and Cook, 1985).

Material parameter, symbol and unit	Values
Density ρ (kg/m^3)	7830
Elastic module E (GPa)	200
Poisson's ratio v	0.29
Specific heat c (J/(kg °C))	502
Thermal conductivity λ (W/(m °C))	38
Expansion coefficient α (°C^{-1})	3.2×10^{-5}
Melting temperature T_m (°C)	1520
A_0 (MPa)	792
B_0 (MPa)	510
N	0.26
C_0	0.014
M	1.03

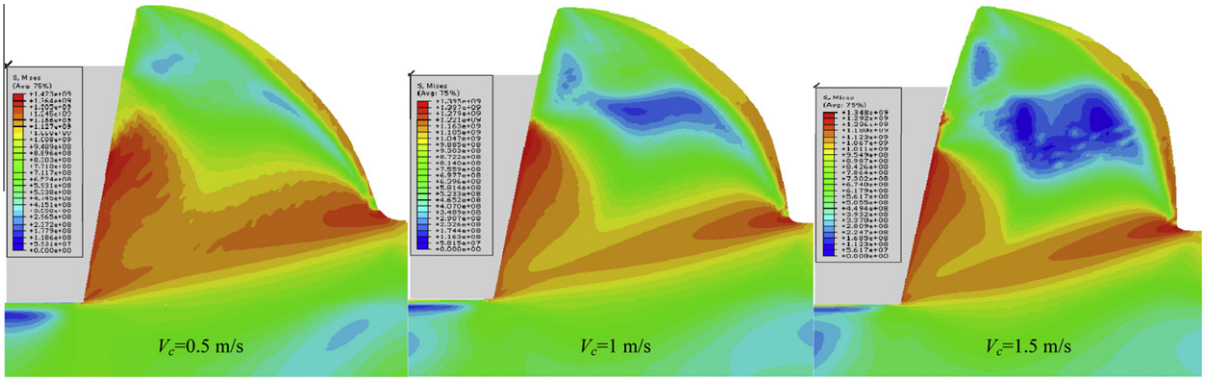

Fig. 8a. The contours of Mises effective stresses at the cutting speeds of 0.5, 1 and 1.5 m/s, respectively.

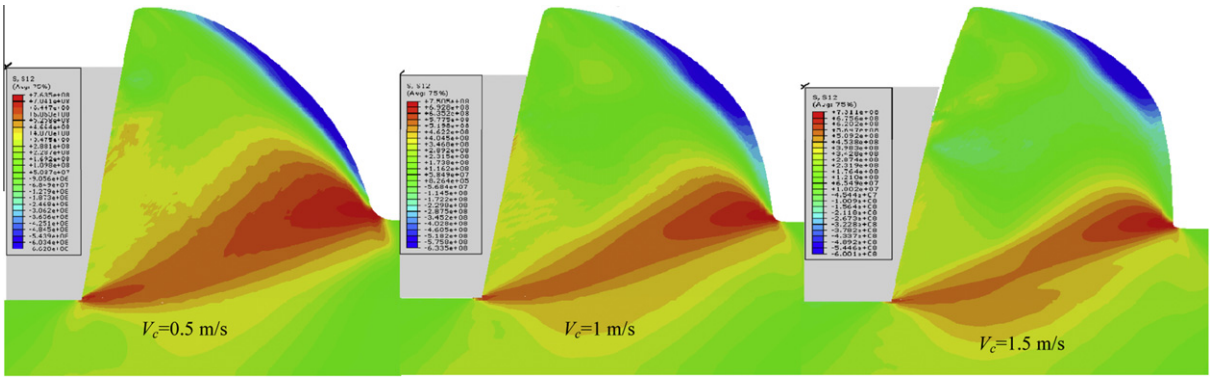

Fig. 8b. The contours of shear stresses at the cutting speeds of 0.5, 1 and 1.5 m/s, respectively.

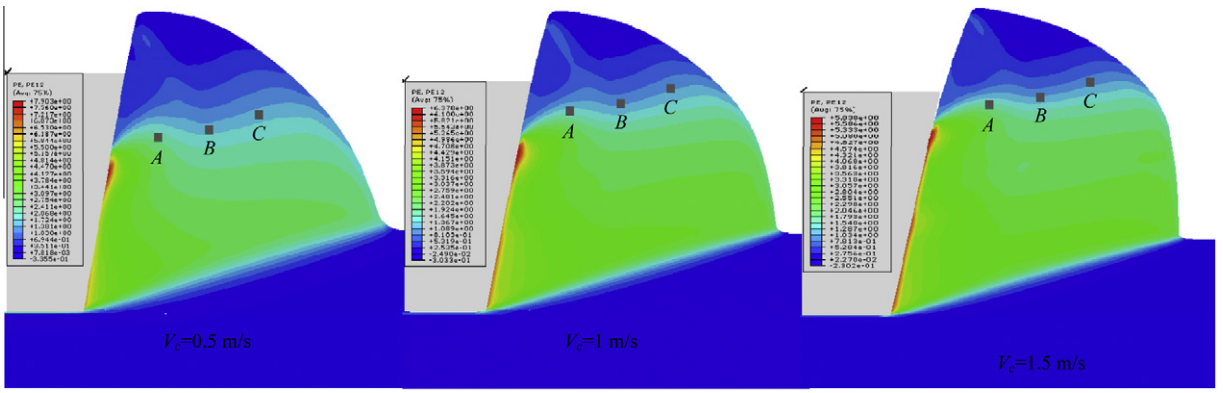

Fig. 8c. The contours of shear strains at the cutting speeds of 0.5, 1 and 1.5 m/s, respectively.

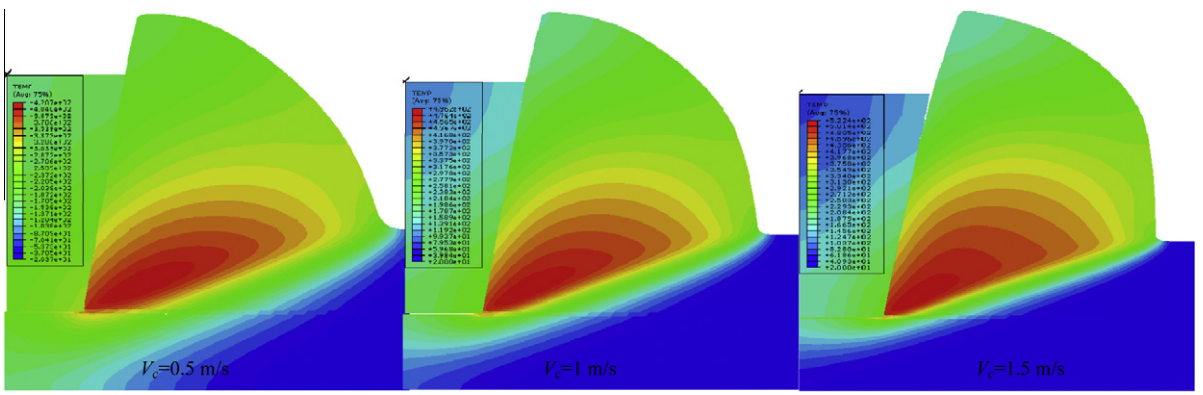

Fig. 8d. The contours of temperatures at the cutting speeds of 0.5, 1 and 1.5 m/s, respectively.

and heat conduction in the cutting process and the heat converted from plastic work causes non-localized thermal softening of materials. Consequently, in the machining process at low cutting speeds, the chip materials of AISI 4340 steel mainly suffer non-localized thermal softening and undergo a steady plastic flow process in which the uniform evolution in stress, deformation and temperature takes place. It is the non-localization plastic flow that leads to the formation of the continuous chips.

Fig. 9 shows the distributions of Mises effective stresses, shear stress, shear strain and temperature at the cutting speeds of 2.5 m/s, 5 m/s and 15 m/s and the cutting distance is 0.5 mm. At present, the shear bands are observed in the chip materials, implying that chip materials undergo strong shear localization deformation which is responsible for the full development of the segment chips as the Komanduri's experimental observations.

Similarly, from Fig. 9a, we can see that the effective stresses distribute in the extensive zone *DEFGHI* which embraces the primary and secondary shear zone and widely extends into the uncut materials. Inside the primary shear zone, the effective stress intensity reaches 1.2 GPa; whereas the intensity of the shear stresses is only 0.55 GPa (Fig. 9b). Therefore, it can be deduced that the normal stresses in the primary shear zone will affect the shear banding formation mechanisms in chip materials even through the shear stress is the primary factor resulting in the shear localization instability of chip materials. Moreover, we note that, in a sizeable zone ahead of the tool tip (Fig. 9b), the intensities of the effective stress and the shear stress have reached 1.3 GPa and 0.74 GPa, respectively. Hence, it is the combined stress at the tool tip that causes the chip materials to separate from the uncut workpiece. The combined stresses in the primary shear zone induce the localization instability of chip material plastic deformation. The shear strain contours in Fig. 9c show that the chip materials undergo evident shear localization instability in the high speed cutting process. The shear strain in the shear bands increase from 3.95, 4.66 to 5.5 as the cutting speeds increase. This suggests that the plastic deformation trends to localization with the increase of cutting speeds. In all cases of high cutting speed, the temperature rise is high localized in the shear bands (Fig. 9d). When the cutting speeds are equal to 2.5 m/s, 5 m/s and 15 m/s, corresponding peak temperatures in shear bands reach 930 °C, 1000 °C and 1200 °C, and the temperatures in the spacing between shear bands come to 140 °C, 200 °C and 270 °C. Clearly, the heat conduction in chip materials in high speed cutting process is not important and the chip material plastic flow in shear bands is adiabatic. Consequently, the adiabatic shear localization instability of chip materials cause the segment chip formation in the high speed cutting process.

Fig. 10 illustrates the relations of Mises effective stress and effective strain for the cutting processes corresponding to above six cutting speeds. The data of each curve are the average value of three points *A*, *B* and *C* as shown in Figs. 8a and 9a. At low cutting speeds, the effective stress reaches sharply peak intensities and then remain constant intensity of about 1.2 GPa, but the effective strain increase steadily which means that the chip materials get into a long range homogeneous plastic flow process. Finally, stress relaxation occurs, that is, the effective stress decreases rapidly and the effective strain remains in different constant strain values. Therefore, at the low cutting speeds, the continuous chip formation is caused by the long range homogeneous plastic flow of chip materials and the cutting process is accompanied by the uniformly steady evolution in stress, deformation and temperature. At the high cutting speed of above 2.5 m/s, the effective stress

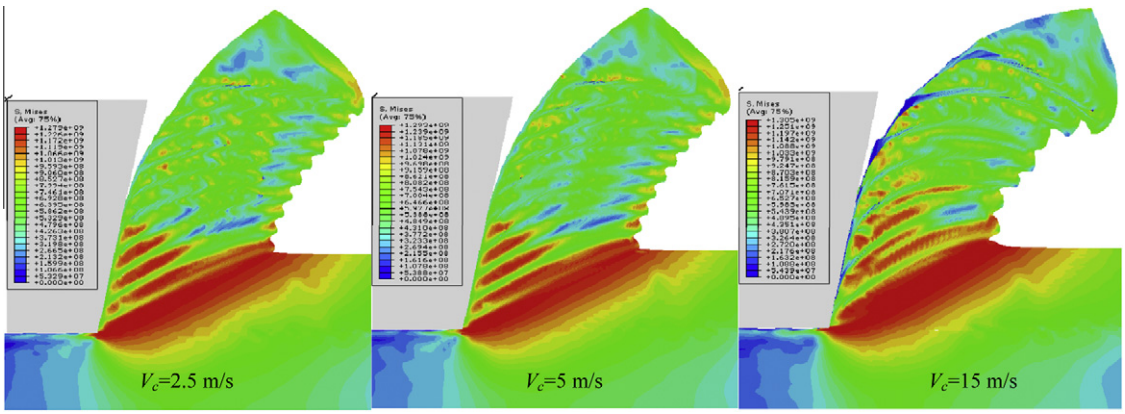

Fig. 9a. The contours of Mises effective stresses at the cutting speeds of 2.5, 5 and 15 m/s, respectively.

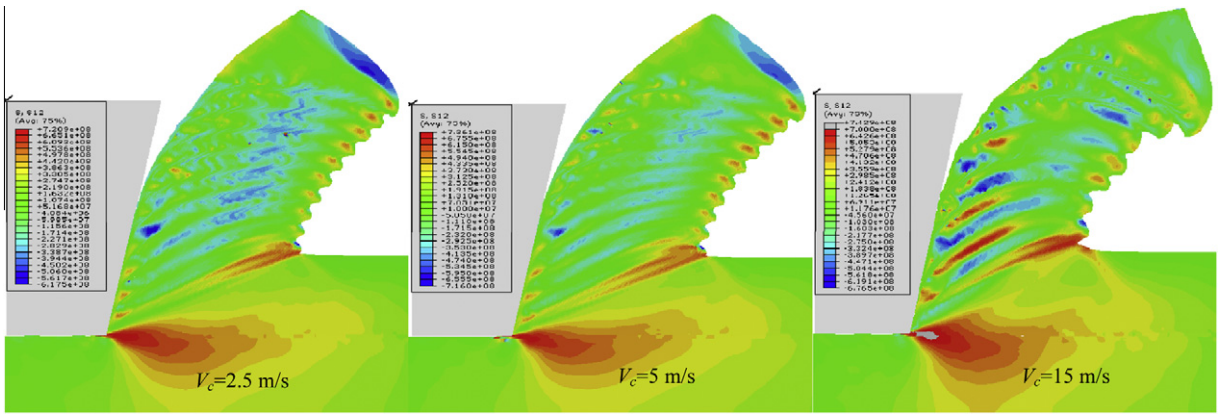

Fig. 9b. The contours of shear stresses at the cutting speeds of 2.5, 5 and 15 m/s, respectively.

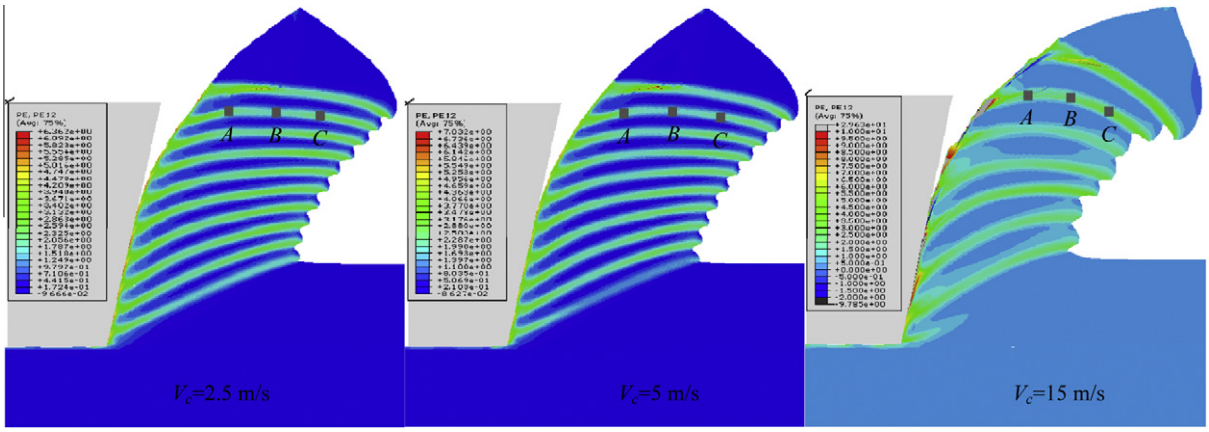

Fig. 9c. The contours of shear strains at the cutting speeds of 2.5, 5 and 15 m/s, respectively.

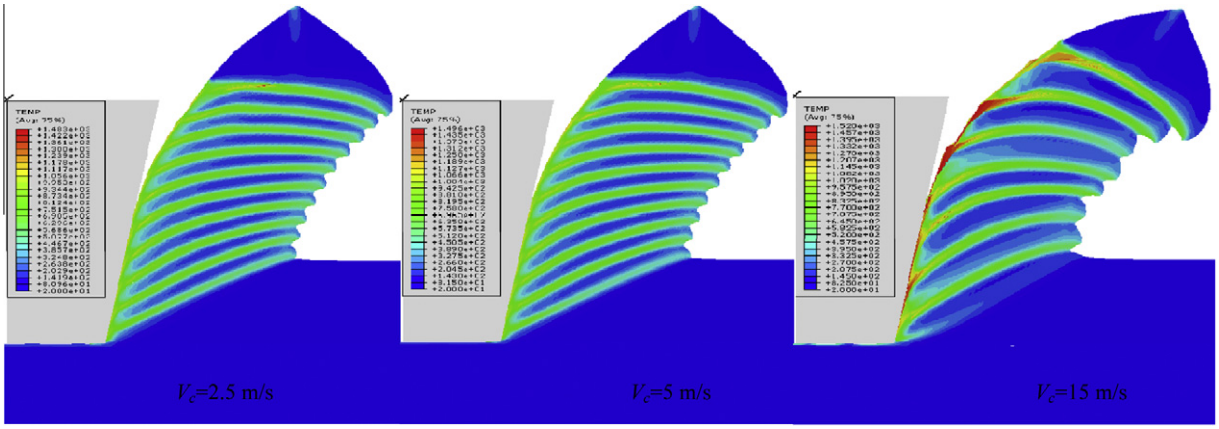

Fig. 9d. The contours of temperatures at the cutting speeds of 2.5, 5 and 15 m/s, respectively.

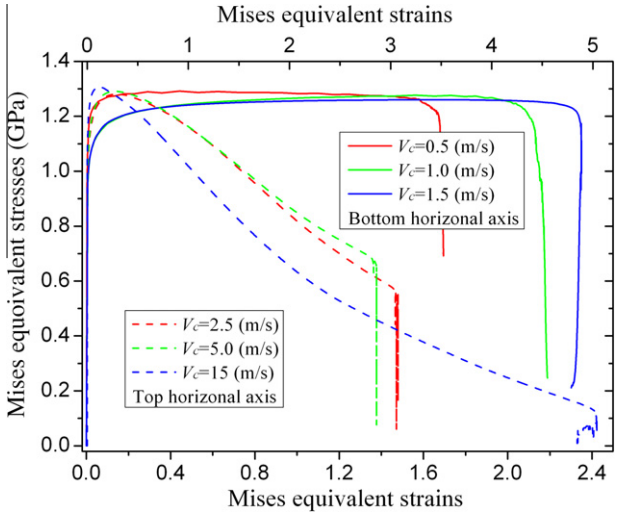

Fig. 10. Variation of the Mises effective stress versus the effective strain when the plastic flow of chip materials occurs in the cutting processes. These curves are obtained by averaging a set of numbers of the three points corresponding to each cutting speed as shown in Figs. 7c and 8c.

decreases sharply from the peak stresses as the effective strain increases, implying that the chip materials undergo the shear localization instability of plastic deformation. For the cases of the cutting speeds of 2.5 m/s and 5 m/s, the chip materials then get into unsteady plastic flow, that is, the stress relaxation in chips occurs; however, when the cutting speed reaches 15 m/s, no stress relaxation appears in the chip materials. Evidently, inhomogeneous evolution in stress and strain takes place in the shear localization instability process.

Fig. 11 provides the predictions of plastic deformation characteristics of chip materials by using the instability phase maps. The strain rates used in these maps are in the orders of 10^4 s^{-1} and 10^5 s^{-1}, which correspond to the low and high cutting speeds, respectively. In each case of the prescribing cutting speeds, we select three elements to determine the intersections of the functions G_1 and G_2 in (18) As shown in the figures of shear stress (Fig. 8c) and (Fig. 9c), these elements A, B, and C are denoted by dark square box. We can see that, in the cases of low cutting speed (Fig. 11a), the intersections fall in the region of steady plastic flow of chip material deformation. Corresponding to the relative low cutting speed, the intersections locate the left side of the region. This is because that the cutting process at relative low speed yields relative large shear stress (Fig. 8b). Therefore, the larger the normal stress intensity is, the more difficult the non-localization instability of chip materials becomes. In the cases of high cutting speeds (Fig. 11b), the intersections are in the region of shear localization instability of chip materials. A clear tendency of the intersection distribution is that they further approach to the left side of the region as the cutting speed is relative low. This is because that the shear stress intensity decreases as the cutting speed reduces (Fig. 9b). So we can deduce that the larger the shear stress intensity is, the easier the shear localization instability of chip materials is.

Fig. 12 provides the ratios of the plastic work power for the 18 points in Fig. 8c and Fig. 9c. We can see that when the cutting speed is below 2 m/s, the ratio of plastic work powers between the compressive deformation and shear deformation

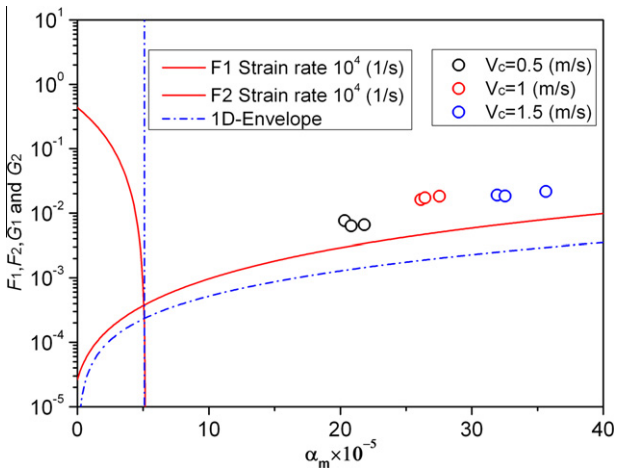

Fig. 11a. The distribution of the nine observed points characterizing the non-localized thermal softening plastic flow of continuous chips in the phase maps, in which the cutting speeds are equal to 0.5, 1 and 1.5 m/s, respectively.

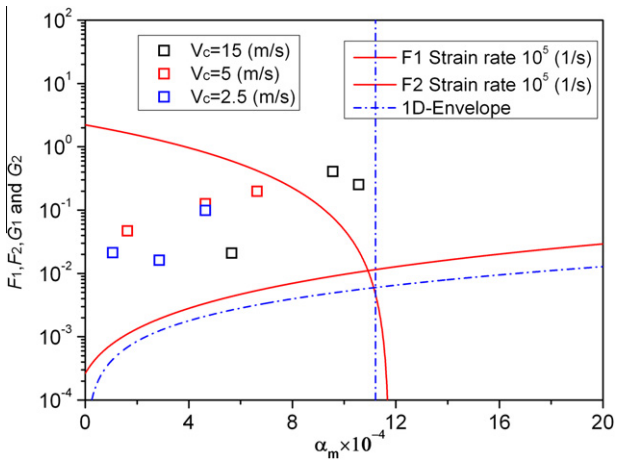

Fig. 11b. The distribution of the nine observed points characterizing the shear localization deformation of discontinuous chips in the phase maps, in which the cutting speeds are equal to 2.5, 5 and 15 m/s, respectively.

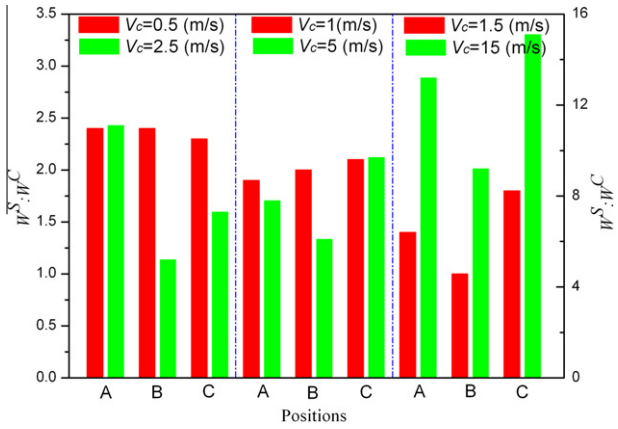

Fig. 12. The ratios between the plastic work power of shear deformation and that of compressive deformation dissipated by continuous and discontinuous chips. The left vertical axis corresponds to the low speed cutting process and the right vertical axis to the high speed cutting process.

W^C:W^S is about in the region of 1:1 to 1:2.5, which are quite larger than the theoretical prediction value 1:4 in the *Case* 3 of previous section. Hence, chip materials undergo homogeneous plastic flow and no shear localization instability occurs. When the cutting speed is above 2.5 m/s, the ratio W^C:W^S is in the region 1:5.2 to 1:15.1. Thus, the shear bands develop in the chip materials. These results are consistent with the theoretical prediction of the instability behaviors of materials under the compression-shear combined stress loading conditions as the *Case* 3 above. Therefore, it can be concluded that the compressive stresses on the primary shear plane strongly affect the formation of chips and the transformation mechanisms between continuous and discontinuous chips in the orthogonal cutting process.

4. Conclusions

It is shown in this study that, under the combined stress loading conditions, the instability mechanisms of materials are quite complex. The knowledge about the instability mechanisms is essential for the understanding of material failure and the improvement of machining technology. Through theoretically quantitative analysis and numerical simulation on the instability mechanisms, we obtain the main conclusions as follows:

1. A general criterion for estimating material instability under combined stresses loading has been established, which describes the instability behaviors of materials with strain hardening, strain rate sensitivity and thermal softening, and considers the effects of heat conduction, normal stresses and strain rates on the instability mechanisms. This criterion indicates that, when the thermal softening effect of material plastic deformation surpasses the work hardening, the material instabilities take place and the mode of material instability is likely to be the adiabatic shear localization, the non-localized thermal softening or long range homogeneous plastic flow. From the criterion we can deduce the instability criteria for some special loading conditions, such as the simple shear, simple tension/compression, non heat conduction effect, dynamic loading and quasi-static loading.
2. Under the combined stress loading conditions, the instability behaviors depend strongly on the loading conditions and are controlled by many influential factors as the shear stress and shear strain rate, normal stress and strain rate and heat conduction. In consideration of energy dissipation, the instability behaviors of materials also depend strongly on the ratios of plastic work dissipated in dilatation deformation to that dissipated in shear deformation. When the plastic work of shear deformation is larger than one third of that of stretching deformation, or is larger than four times of that of shrinking deformation, the shear located instability is possible; otherwise, non-localized thermal softening instability or long range homogeneous plastic flow would occur. Therefore, the shear localized instability is much more sensitive to the compressive stress than the tension stress.
3. The influences of strain rate sensitivity on material instable mechanisms closely related to the loading conditions of combined stresses. In the case of tension-shear combined stress loading, the shear localization instability is always possible; however, under the loading conditions of compression-shear combined stresses, both shear localization instability and non-localized thermal softening instability are possible when the shear strain rates vary.
4. In the orthogonal cutting process of AISI 4340 steel, the normal stresses affect strongly the chip formation and transformation mechanisms between continuous and discontinuous chips. As the cutting speed is below 2 m/s, long range homogeneous plastic flow yields continuous chips. As the cutting speed is above the value, shear localization instability causes the shear bands in chip materials and the shear localization instability results in the formation of discontinuous chips. The transformation between the continuous and discontinuous chips depends on the ratios of plastic work power of the compressive deformation with that of shear deformation.

Acknowledgements

The authors acknowledge financial supports from the National Nature Science Foundation of China (Grant No. 10972227) and the National Key Basic Research Program of China (Grant No. 2009CB724401).

References

Anand, L., Kim, K.H., Shawki, T.G., 1987. Onset of shear localization in viscoplastic solids. J. Mech. Phys. Solids 35, 407.
Argon, A.S., 1973. The Inhomogeneity of Plastic Deformation. Am. Soc. Metals, Metals Park, Ohio (Chapter 7).
Bai, Y.L., 1982. Thermo-plastic instability in simple shear. J. Mech. Phys. Solids 30, 195.
Bäker, M., Rösler, J., Siemers, C., 2002. A finite element model of high speed metal cutting with adiabatic shearing 80, 495.
Batra, R.C., Liu, D.S., 1990. Adiabatic shear banding in dynamic plane strain compression of a viscoplastic material. Int. J. Plast. 6, 231.
Borg, U., 2007. Strain gradient crystal plasticity effects on flow localization. Int. J. Plast. 23, 1400.
Burns, T.J., Davies, M.A., 2002. On repeated adiabatic shear band formation during high-speed machining. Int. J. Plast. 18, 487.
Burns, T.J., Trucano, T.G., 1982. Instability in simple shear deformation of strain-softening materials. Mech. Mat. 1, 313.
Chen, K.W., Lin, J.F., 2010. Investigation of the relationship between primary and secondary shear bands induced by indentation in bulk metallic glasses. Int. J. Plast. 26, 1645.
Clifton, R.J., 1980. Report to the NRC Committee on Material Responses to Ultrasonic Loading Rates. NMAB-356, 129.
Culver, R.S., 1973. In: Rhode, R.W. (Ed.), Metallurgical Effects at High Strain-rates. Plenum Press, New York.
Di Rado, H.A., Beneyto, P.A., Mroginski, J.L., Awruch, A.M., 2009. Influence of the saturation–suction relationship in the formulation of non-saturated soils consolidation models. Math. Comput. Model. 49 (5-6), 1058.
Farrokh, B., Khan, A.S., 2009. Grain size, strain rate, and temperature dependence of flow stress in ultra-fine grained and nanocrystalline Cu and Al: Synthesis, experiment, and constitutive modeling. Int. J. Plast. 25, 715.
Fressengeas, C.F., Molinary, A., 1987. Instability and localization of plastic flow in shear at high strain rates. J. Mech. Phys. Solids 35, 185.
Hashiguchi, K., Tsutsumi, S., 2007. Gradient plasticity with the tangential-subloading surface model and the prediction of shear-band thickness of granular materials. Int. J. Plast. 23, 767.
Hortig, C., Svendsen, B., 2007. Simulation of chip formation during high-speed cutting. J. Mater. Process. Technol. 186, 66.
Jiang, M.Q., Dai, L.H., 2009. On the origin of shear banding instability in metallic glasses. J. Mech. Phys. Solids 57, 1267.
Johnson, G.R., Cook, W.H., 1983. A constitutive model and data for metals subjected to large strains, high strain rates and high temperatures. In: Proceedings of the Seventh International Symposium on Ballistics, p. 541.
Johnson, G.R., Cook, W.H., 1985. Fracture characteristic of three metals subjected to various strains, strain rates, temperatures and pressures. Eng. Fract. Mech. 21, 31.
Kobayashi, M., 2010. Analysis of deformation localization based on proposed theory of ultrasonic wave velocity propagating in plastically deformed solids. Int. J. Plast. 26, 107.
Komanduri, R., 1982. On the catastrophic shear instability in high-speed machining of an AISI 4340 steel. J. Eng. Indust. 104, 121.
Kuroda, M., 1996. Roles of plastic spin in shear banding. Int. J. Plast. 12, 671.
Kuroda, M., Tvergaard, V., 2007. Effects of texture on shear band formation in plane strain tension/compression and bending. Int. J. Plast. 23, 244.
Liang, R., Khan, A.S., 1999. A critical review of experimental results and constitutive models for BCC and FCC metals over a wide range of strain rates and temperatures. Int. J. Plast. 15, 973.
Merchant, M.E., 1945. Mechanics of the metal cutting process. I. Orthogonal cutting and a type 2 chip. J. Appl. Mech. 16, 267.
Molinari, A., Musquar, C., Sutter, G., 2002. Adiabatic shear banding in high speed machining of Ti–6Al-4V: experiments and modeling. Int. J. Plast. 18, 443.
Mroginski, J.L., Etse, G., Vrech, S.M., 2011. A thermodynamical gradient theory for deformation and strain localization of porous media. Int. J. Plast. 27, 620.
Pan, J., 1983. Perturbation analysis of shear strain localization in rate sensitive materials. Int. J. Sol. Struct. 19, 153.
Niordson, C.F., Tvergaard, V., 2005. Instabilities in power law gradient hardening materials. Int. J. Solids Struct. 42, 2559.
Özel, T., Altan, T., 2000. Process simulation using finite element method—prediction of cutting forces, tool stresses and temperatures in high speed flat end milling. J. Mach. Tools Manuf. 40, 713.
Paul et al, 2009. On twinning and shear banding in a Cu-8 at.% Al alloy plane strain compressed at 77 K. Int. J. Plast. 25, 1588.
Piispanen, V., 1948. Theory of formation of metal chips. J. Appl. Mech. 19, 876.
Recht, R.F., 1964. Catastrophic thermoplastic shear. J. Appl. Mech. 31, 189.
Shaw, M.C., 1984. Metal Cutting Principles. Clarendon Press, Oxford.
Sorenson, H.K., Inc., 1996, ABAQUS/Explicit User's Manual, ver.5.6, Providence, RI.
Staker, M.R., 1981. The relation between adiabatic shear instability strain material properties. Acta Metall. 4, 683.
Sun et al, 2009. Predicting failure modes and ductility of dual phase steels using plastic strain localization. Int. J. Plast. 25, 1888.
Sutter, G., Faure, L., Molinari, A., Deiime, A., Dudzinski, D., 1997. Experimental analysis of the cutting process and chip formation at high speed machining. J. Phys. IV, France 7, 33.
Walker, T.J., Shaw, M.C., 1969. Proc. 10th Int. Mach. Tool Des. and Res. Conf. Pergamon Press, Oxford, 291.
Xie, J.Q., Bayoumi, A.E., Zbib, H.M., 1998. FEA modeling and simulation of shear localized chip formation in metal cutting. J. Mach. Tools Manuf. 38, 1067.
Zbib, H.M., Jubran, J.S., 1992. Dynamic shear banding: a three-dimensional analysis. Int. J. Plast. 8, 619.